Energy &
Environmental Science

RSC Publishing

REVIEW

View Article Online
View Journal

Cite this: DOI: 10.1039/c3ee41860j

The identification, characterization and mitigation of defect states in organic photovoltaic devices: a review and outlook

John A. Carr and Sumit Chaudhary*

Received 31st May 2013
Accepted 29th August 2013

DOI: 10.1039/c3ee41860j

www.rsc.org/ees

In any microelectronic device, fundamental physical parameters must be well understood for successful electronic optimization. One such prominent parameter is energetic trap states, which are well-known to plague amorphous or otherwise impure semiconducting materials. Organic semiconductors are no strangers to such states and their electronic properties are evidently tied to these defects. Herein, this article discusses the identification, characterization and mitigation of bandgap residing trap levels in organic photovoltaic devices. A compilation of select studies to date is given and a general outlook is proposed. Organic photovoltaic materials are depicted as multiple trap-level systems with a seemingly continuous distribution of electronic states throughout the bandgap. Some elucidations as to the origins of these electronic states as well as recent works centered on defect removal are also presented.

Broader context

In the search for clean, sustainable energy sources, organic photovoltaics have emerged as a promising technology. These devices represent a lightweight, flexible, low-cost and environmentally benign power source, which has great potential in many applications. However, before large-scale commercialization is possible, these devices must first be efficient, reproducible and stable solar converters. Like several other photovoltaic technologies, each of these three – efficiency, reproducibility and stability – are limited in OPVs by the presence of electronic defects within the semiconductor band-gap. The reduction of such states by even an order of magnitude has the potential to nearly double photovoltaic conversion efficiency. As an effort in this direction, this review examines these defects, their sources, how they might affect the OPV electronic properties and potential methods of mitigation.

1. Introduction and background

The last decades have witnessed a shift in the world views of the energy sources which sustain our industries, homes and transportation. To date, the fossil fuels have been staple power generators; however, many have begun to question the impact of burning resources such as coal and oil on both human and environmental health. This, coupled with pushes to achieve energy independence with long-term sustainable sources, has spurred extensive research into alternative energies. The most promising, low-carbon sources include nuclear, wind, geothermal and solar – each with distinct advantages. Though a likely solution to the energy needs consists of a diverse combination of the above, this review focuses on specifics of the latter: solar power. Photovoltaic devices have become popular for many applications owing to their relative small scale (*e.g.* can be incorporated into many products), independence from large infrastructure (*e.g.* suitable for off-grid locations) and decentralization (*e.g.* the energy source does not need to be transported).

Today, the terms 'solar cell' and 'solar panel' typically refer to commercially available arrays based on inorganic materials such as silicon or cadmium telluride. However, within the research community, organic materials have emerged as strong candidates for the next generation of devices. These materials offer numerous advantages, including thin film thickness, lights weights, mechanical flexibilities, a relative ease of processing and a lower environmental impact (*e.g.* low energy payback time and low levels of anthropogenic emissions).[1] Most notable are the latter two. Low-temperature, solution based fabrication opens the door for large scale roll-to-roll production. This has the potential to greatly reduce commercial manufacturing costs, enabling a wider scale of affordability and distribution with less environmental impact than the more traditional photovoltaic technologies. Of course, in order to become more commercially feasible, organic photovoltaic (OPV) cells must first be efficient, stable and reproducible solar converters.

OPV research has been ongoing for many years. Numerous important breakthroughs have gated today's progress and the last decade in particular has seen a rapid improvement in OPV

Iowa State University, Department of Electrical and Computer Engineering, 2124 Coover Hall, Ames, Iowa 50011-3060, USA. E-mail: sumitc@iastate.edu; Tel: +1 (515) 294 0606

performance. The first OPV devices consisted of a single-layer organic semiconductor sandwiched between two electrodes. Photons incident on the organic material were absorbed, which, owing to a low dielectric constant and small Bohr radius of carriers, generate a bound electron/hole pair.[2] Within the bulk, the electric field was insufficient for exciton dissociation, thus the power conversion efficiency (PCE) was severely limited as most photogenerated charges were lost to recombination. In response, Tang demonstrated a bilayer structure comprising a planar stack between an organic donor and acceptor.[3] This p–n heterojunction-like device produced a large dissociation field at the material junction and gave a PCE of nearly 1%.[3] However, with the typical exciton diffusion length (*ca.* 10 nm) an order of magnitude smaller than the thickness required for high optical absorption (*ca.* 100+ nm), many excitons were unable to reach the separation interface and were still lost. Thus, Halls *et al.* and Yu *et al.* then introduced the bulk heterojunction (BHJ) concept; a blended film comprised of a bulk mixture between donor and acceptor materials.[4,5] This bulk blend generates dissociation interfaces at a phase segregation nearing the exciton diffusion length, while still allowing for sufficient optical thickness. The structure pushed single junction PCEs to several percent, a number which in recent days is approaching 10%.[6]

Though the field has impressively progressed over the last several years, the Schockley–Queisser PCE limit of a single junction BHJ OPV has been calculated at *ca.* 23%.[7] This highlights that extensive bottlenecks still exist. Energy level misalignment, inadequate light trapping, poor exciton diffusion, recombination and low carrier mobilities have been cited as the top deficiencies limiting device performance.[7] Through the efforts to alleviate these bottlenecks, many of the latest breakthroughs have come from the development of new materials. Each with improved bandgaps and tuned energy level offsets to improve absorption, open circuit voltage, charge dissociation, *etc.* However, no matter the material, fundamental physical parameters will remain important, and understanding their role in OPV performance is crucial in further optimizing this promising technology.

2. Defects: background, definition of terms, *etc.*

One such underlying physical parameter is the presence of material defects and the mid-gap energy states they create. When speaking of organic semiconductors, the highest occupied molecular orbital (HOMO) and lowest unoccupied molecular orbital (LUMO) are commonly referenced. These orbitals are often likened to the valence and conduction bands of inorganic materials and, similarly, are separated by a bandgap. Within this energy gap, it is well known that both shallow- and deep-level states can be present (Fig. 1), painting a picture of energetic disorder in OPV materials. Generally speaking, the origins of these trap states are described by two broad categories: extrinsic and intrinsic.[8] Extrinsic traps stem from extrinsic defects, such as chemical impurities introduced during material synthesis, device fabrication or exposure to oxygen or moisture.[8–18] External bias-stress and an

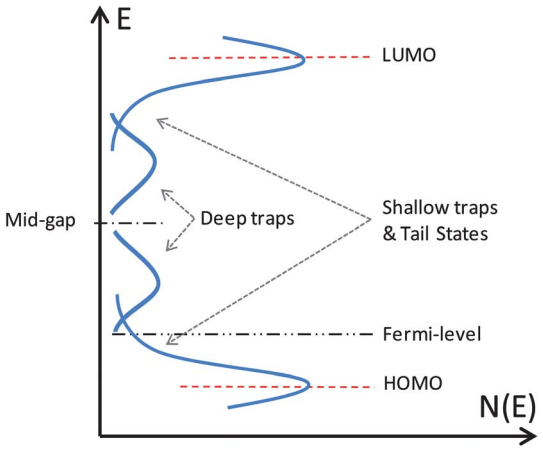

Fig. 1 Simplified model conceptually illustrating the density of states in an organic material.

electrochemical process involving oxygen and electrical biasing have also been shown to generate metastable mid-gap states – which are extrinsic by nature.[19,20] Extrinsic, chemical defects can be further described as either bound or unbound, differentiating impurities that are chemically appended from those that are not.[21] Intrinsic traps stem from intrinsic defects. These defects arise from the morphological disorder inherent in the amorphous nature of a typical organic film.[2,22–25] Morphological defects can be described as either noncovalent or covalent.[2] The former refers to energetic entities which slightly perturb surrounding energy levels, generating states [typically] shallower in the bandgap.[26] Owing to their weak effects, no covalent bonds are altered. This type of disorder is common in molecular organic semiconductors.[2] In contrast, the latter refers to defects which cause higher energy perturbations, affecting covalent bonds and generating levels [typically] deeper in the gap.[27] This type of disorder is common in π-conjugated organic semiconductors.[2,27] Of course, not all defects will lead to electroactive mid-gap states. Some may yield energy states within the carrier bands themselves,[24] and are of less interest to the review at hand. Yet, it is those imperfections which produce bandgap residing states, both shallow and deep, that are of great importance to OPV device physics and performance.

It is well known that such defects can have profound effects on physical operation in inorganic devices.[28–30] Thus, it comes with no surprise that we should expect similar effects on OPV performance, significantly contributing to the abovementioned deficiencies. It has even been said that defects completely control the electronic properties of amorphous and polycrystalline organic materials,[27] truly highlighting the need for an in-depth understanding of these states. Defects are known to introduce recombination centers, charged point sites or both. If present in appreciable concentrations, recombination centers can contribute to free carrier loss through trap-assisted recombination, especially if the trap is spatially located at or near a donor–acceptor interface.[31–33] Charged defects are known to greatly affect the electrostatic potential throughout the device,[8] which can be detrimental to carrier mobility and inhibit

transport,[21,27] as well as retard the probability of charge separation and promote the likelihood bimolecular recombination.[34] Further, bulk charges have been linked to the quenching of photogenerated excitons, indicating the presence of charged defects may strongly limit the diffusion length of this important quasiparticle.[21,27] Energetic trap sites can also pin the Fermi-level deep within the bandgap, greatly suppressing the built-in field.[35] In a solar cell device, each of these can yield losses in short circuit current density (J_{sc}), open circuit voltage (V_{oc}) and/or fill factor (FF); hindering the overall PCE. Further, the enhancement of inherent traps or the creation of new bands during device operation (*e.g.* through light or oxygen exposure), largely affects OPV stability and may greatly contribute to the long-term degradation of these devices.[36,37] On the other hand, some aspects of these unintentional defects states may be beneficial to OPV performance.

As such, this has inspired Wang *et al.* to ask "Do the defects make it work?".[26] The typical organic semiconductor employed in OPV devices has a bandgap nearing 2 eV. This strongly limits the intrinsic carrier concentration to 1×10^3 to 1×10^7 cm^{-3}.[2,27] However, the actual carrier density can be substantially higher. For example, common π-conjugated polymers have a concentration reaching 1×10^{15} to 1×10^{19} cm^{-3}, some 8 to 16 orders of magnitude higher than the estimated intrinsic density.[26,38–41] These extra carriers originate from both structural and extrinsic defects which produce electronic states near a band edge.[2] Oxygen and moisture, in particular, have been identified as sources of p-type doping, especially if the exposure is in the presence of light.[9,10,13,42–48] Controlled doping has proven to be an important parameter for inorganic devices and, albeit typically unintentional, these defects may be just as advantageous for OPVs. Most notably, these excess concentrations may vastly alter carrier conductivity as well as the electric field at the donor–acceptor interface,[2,9,26,27,49–51] improving charge transport and exciton dissociation while lowering recombination probability at the interface. Of course, as the dopant carrier moves into the more delocalized states, it leaves behind a localized site of opposite charge, unavoidably generating a coulomb trap. As stated above, such charged states can have profound effects on electrical properties, and thereby, a tradeoff is formed.[9,50]

Nonetheless, good or bad, defect states in plastic solar cells must be well understood. Thus, their identification, characterization and potential mitigation or enhancement remain important areas of research. The first, *identification*, represents the need to profile the complete trap density of states (tDOS) throughout the bandgap of OPV materials. As is typical in amorphous thin-films, multiple trap bands may exist – highlighting the importance of rigorous profiling techniques to ensure all prominent bands are known. The second, *characterization*, is the determination of the physical characteristics of these trap bands and their affect(s), whether it be positive or negative, on solar cell performance. Among many characteristics, one might be interested in the energetic location, concentration, disorder spreading, spatial location, type of carrier (majority or minority) trapped and capture/emission coefficients. The last, *mitigation* or *enhancement*, refers to an end goal of reducing defects states that negatively influence OPV performance while augmenting states that have a positive effect. Though it will be impossible to completely rid OPV materials of detrimental defects, reducing trap states by even an order of magnitude[32] and gaining better control of the impurity based doping will be highly beneficial to performance.

As a step towards realizing this goal, this report presents a review of select studies centered on defects in OPV devices. Our intention is to highlight the progression of trap band identification, characterization and mitigation to date and give a general view of its current state. Trap profiling in neat materials will first be examined, followed by that in blended systems. Trap effects on OPV performance as well as thoughts on trap origins can found throughout. The article concludes with a brief summary and proposed outlook. In an effort to give a general understanding as to the employed measurements, their introductory concepts, equations and relevant citations are provided in an Appendix.

A note on nomenclature: relatively shallow impurities are routinely introduced into inorganic materials to manipulate free-carrier concentrations. In such a case, these states are referred to as donors (*i.e.* readily donate an electron to the conduction band to dope n-type) or acceptors (*i.e.* readily accept an electron from the valence band to dope p-type).[52] Herein, we adopt this nomenclature to describe the extrinsic behavior of OPV materials. N_A will refer to those relatively shallow levels, which give an apparent p-doping. Similarly, relatively deep impurities can be considered either donor-like (trap-neutral when electron filled and positively charged when empty) or acceptor-like (trap-neutral when hole filled and negatively charged when empty).[52] Herein, this nomenclature is adopted and such deep trap levels are marked N_T.

3. Identification and characterization: neat material systems

3.1. General depiction

As a starting point, we look at photothermal deflection spectra (PDS) from Goris *et al.* to understand wavelength dependent absorption, and thereby, the general depiction of the midgap tDOS in common OPV materials.[53] The spectra of neat poly(3-hexylthiophene) (P3HT), neat poly(*p*-phenylene vinylene (PPV), neat [6,6]-phenyl-C61-butyric acid methyl ester) ($PC_{60}BM$) and blends thereof are shown in Fig. 2. For the time being, we will concentrate on the neat materials, but later revisit the blend spectra. The three materials listed are extensively studied *model* OPV systems and will be heavily concentrated on in this article. The PDS spectra shown in Fig. 2 establish the generally accepted picture of the molecular orbitals and energetic DOS. Weak absorption at lower energies, a rapid increase at moderate energies and relatively strong absorption at higher energies is seen. This is in accordance with molecular orbitals that are Gaussian in nature, broadening of which introduces a distribution of shallow defects that trail into more localized states deeper in the gap. Turning to other works, some substantiation of this picture can be found.

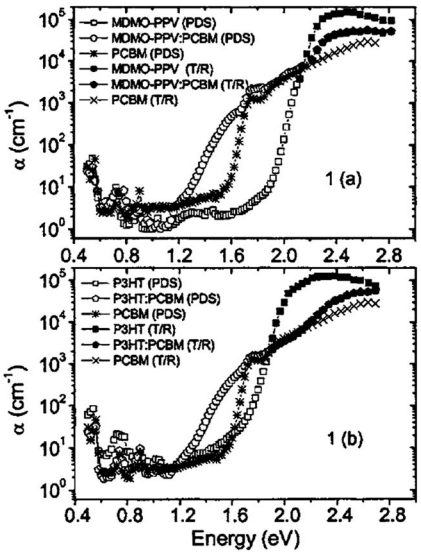

Fig. 2 (a) PDS-spectrum of dropcast layers of MDMO-PPV (square), PCBM (star) and MDMO-PPV:PCBM (80 wt%) (pentagon). (b) PDS-spectra of dropcast layers of P3HT (square), PCBM (star) and P3HT:PCBM (66.66 wt%) (pentagon). The full symbols (PCBM = star) correspond to data obtained with transmittance and reflectance measurements. Reprinted with permission from ref. 53. Copyright [2006], American Institute of Physics.

In acceptor materials, this general depiction is readily substantiated by earlier optical experiments on C_{60} and C_{70} fullerites.[54,55] Again, distinct absorption in the sub-gap regime was observed and identified as an Urbach tail (shallow states) leading into localized electronic levels (deeper states). In donor materials, a more thorough substantiating view can be offered through thermally stimulated current (TSC) measurements (refer to Appendix section 8.1 for details).[56] In the cited work, an indium tin oxide (ITO)/P3HT/aluminum (Al) structure was studied.[56] As shown in Fig. 3, the resulting TSC profile identifies two prominent peaks in the energetic tDOS. The first, low temperature peak (93 K) represents relatively shallow levels, likely tail states extending from the Gaussian orbital. The second, high temperature peak (200 K) represents deeper states, likely more localized trap levels. This illustrates a tDOS much like that of Fig. 1 and is in support of the PDS data.

Clearly, the general depiction shows a distribution of bandgap residing states in both pure donor and pure acceptor materials. In the subsequent subsections, we will further detail and quantify these shallow and deep trap states and highlight their origins.

3.2. Levels in donor materials

3.2.1. Relatively shallow activation energies. To begin the more detailed discussion, we focus first on shallow traps in neat donor materials. The low temperature TSC peak above was confirmed and further resolved in 2008.[57] Here, ITO/poly(3,4-ethylenedioxythiophene) poly(styrenesulfonate) (PEDOT:PSS)/P3HT/Al devices were studied.[57] A low temperature peak around 85 K (105 meV) with a shoulder around 50 K (50 meV) was found (Fig. 4a, black line). The 85 K peak is in good agreement with the prior TSC work (93 K), however, the aforementioned 200 K peak was not reproduced.[57] A similar finding was also noted through drive-level transient spectroscopy (DLTS; refer to Appendix section 8.6 for details), where a single trap level with an activation energy of *ca.* 87 meV was revealed but, again, no deeper band was seen.[58] Interestingly, Schafferhan's shallower 'shoulder band' was also not noted in the DLTS work. In any

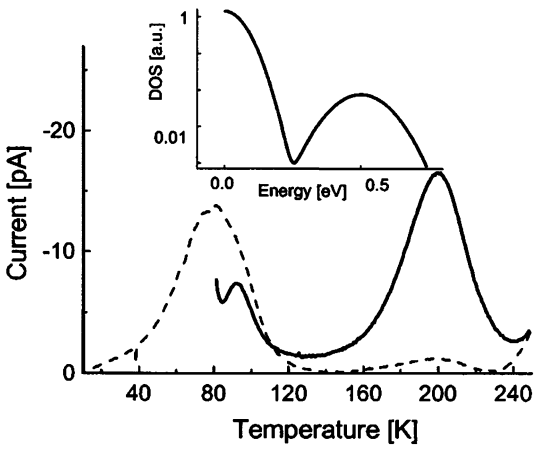

Fig. 3 TSC signal from a thin film of P3HT sandwiched between an ITO and aluminum electrode for the case of temperature of trap filling 77 K (solid line) and 4 K (dashed line). Inset shows the energy dependencies of the DOS. Reprinted with permission from ref. 56. Copyright [2003], American Institute of Physics.

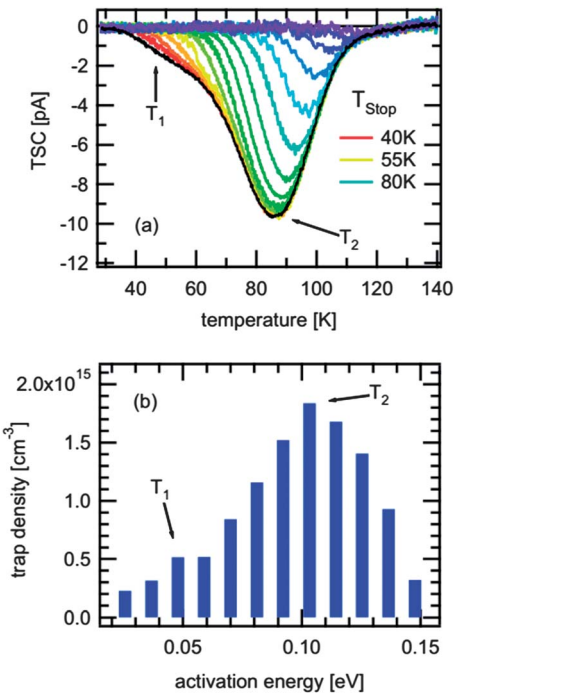

Fig. 4 (a) Main runs of the different T_{start}–T_{stop} cycles, as well as the conventional TSC spectrum (black curve), revealing two trap states T1 and T2 and (b) the resulting DOOS distribution. Reprinted with full permission from ref. 57. Copyright [2008], American Institute of Physics.

case, Schafferhans *et al.* estimate the total trap density in the studied energy regime to be *ca.* 1.0×10^{16} cm^{-3}.[57] To further quantify and construct a resolved profile of the tDOS (Fig. 4b), the authors then applied the so-called fractional T_{start}–T_{stop} TSC technique (Fig. 4a, colored lines; refer to Appendix section 8.2 for details). Clearly seen in the resolved factional data is the overlap of two Gaussian-like distributions, indicating two prominent bands in a continuous distribution of relatively shallow trap states.

Shallow activation levels in unblended donors have also been directly observed through capacitance *versus* voltage (CV) measurements (refer to Appendix section 8.4 for details).[13] It should be noted that the CV measurement is sensitive only to mobile charges. Herein, complete ionization is not assumed and this CV measured quantity is referred to as the 'ionized acceptor density' (N_A^-). This value should be considered, at the least, a lower limit of the total shallow impurity concentration. As mentioned in Section 2, defects tend to give OPV materials an apparent p-type doping. With moderate dopings, Fermi-levels are in the range of a few hundred meV above the HOMO. This, coupled with cathode work functions that are several hundred meV lower, promotes the formation of a Schottky barrier at the organic–cathode junction.[59] The existence of such an interface in neat P3HT diodes was evidently shown by Dennler *et al.*, and thereby, the authors demonstrated the ability to leverage depletion capacitance techniques on these systems to study bandgap residing states. In Dennler's work, the charge carrier density as per air exposure was monitored through CV measurements (Fig. 5).[13] The group found the ionized acceptor density evolved from 5.0×10^{16} to 1.0×10^{17} cm^{-3} throughout the exposure experiment.[13] The as-cast density is in the same range as that predicted by the TSC measurements,[57] again showing a strong presence of shallow levels. The evolution of the concentration through air exposure supports the claim that oxygen and moisture give rise to a p-type doping and will be later revisited in Section 3.4.

Other CV works can be explored for comparison. One such work was recently provided by Li *et al.*[60] The group studied CV characteristics at various frequencies on a ITO/PEDOT:PSS/P3HT/Al structure. An ionized impurity concentrations in the range of 6 to 10×10^{14} cm^{-3} was found,[60] significantly lower than that of Dennler *et al.*[13] Though the exact reason for this large difference is unknown, we suspect several likely contributors. Simply, variations in air exposure could cause this noted difference. However, one must also remember structural imperfections as well as other chemical impurities can contribute to the shallow level concencetration.[2] When comparing the fabrication of each group's devices, we find a film thickness of *ca.* 1 μm for Dennler and *ca.* 5 μm for Li.[13,60] Thicker films dry more slowly and slower drying is known to improve reduce structural disorder.[61] Thereby the apparent p-type doping may be reduced. This gives a good introduction to the effects simple processing parameters can have on energetic defect states.

CV measurements have also been used to identify shallow states in PPV based diodes (Fig. 6) – an ITO/PPV/Al structure was studied.[62] The measurements were taken between −5 and $3V_{DC}$; the employed frequency is not known.[62] A quantification for

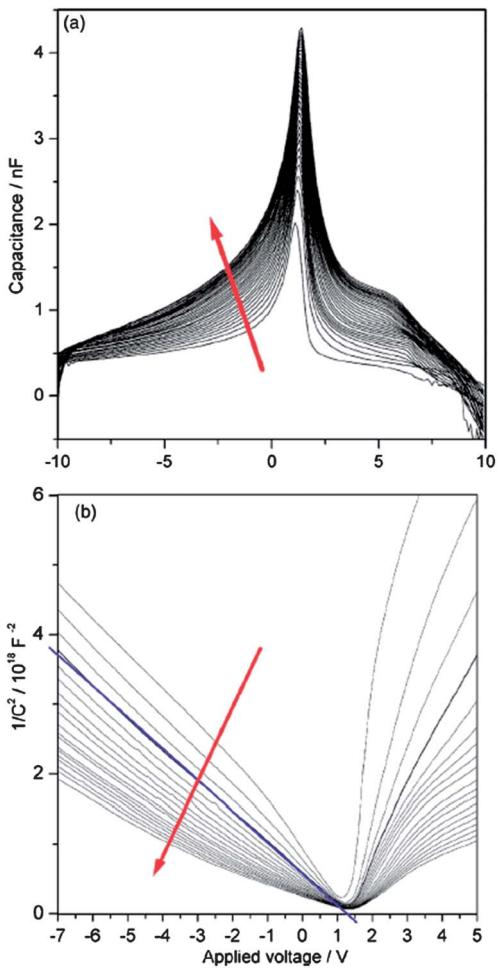

Fig. 5 (a) Capacitance C and (b) $1/C^2$ of an ITO/P3HT/Al diode recorded at 1 kHz every 2 min in air *versus* the applied voltage V. The arrows indicate increasing time. The solid line in (b) is a linear fit of one intermediate curve. Reprinted with full permission from ref. 13. Copyright [2005], American Institute Physics.

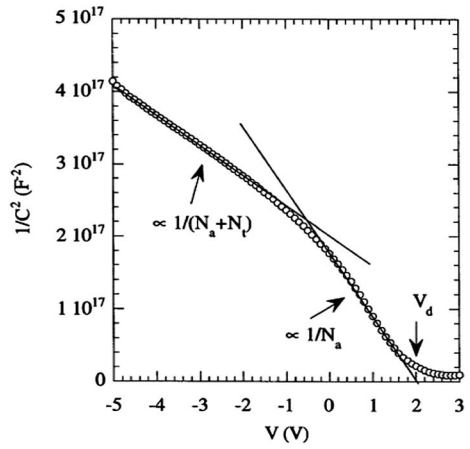

Fig. 6 Inverse capacitance squared, $1/C^2$, against applied bias, V_{appl}, of an ITO/PPV/Al device.

N_A^- was not given, but can be estimated in the range of 5×10^{16} cm^{-3} if we are to assume a nominal device area. This is in line with typically reported values.

Clearly, shallow states in neat donors are present. Fractional TSC measurements show these states to be distributed in energy, while CV indicates these states [at least partially] ionized to give rise to an appreciable amount of mobile charges. Moving forward, we wish to elucidate the states deeper in energy. Such states are subtly seen in Fig. 6.

Upon further examination of Fig. 6, one notes a break in the Mott–Schottky (MS) slope at *ca.* $-0.75V_{DC}$. In fact, Dennler *et al.* as well as Li *et al.* also observed this dual slope. In the former (Fig. 5), the authors imputed the break to an inhomogeneous doping profile induced by the fabrication process.[13] This is a reasonable attitude considering a spatial change (increase) in N_A^- would induce such a slope change. Li *et al.*, however, have indicated this may be the result of a non-uniform spatial doping *or* may represent the presence of energetically deep trap band(s).[60] The latter highlights a second, important interpretation, which has a basis in deep-trap-rich materials.[63] The formalization of such an interpretation was given by Kimerling and is summarized in Appendix section 8.4.[64] Campbell *et al.* have taken this interpretation and asserted the break stems from deep trap contributions. This gives the indication that levels with a relatively deeper activation energy are present, which, because of the prominent decrease in the MS slope, are acceptor-like such that $N_T > N_A^-$.[62] This interpretation is in line with the general 'shallow + deep trap' depiction of Section 3.1, giving some corroboration to the authors' theory. The next section aims to focus on these deep states in donor materials.

3.2.2. Relatively deep activation energies. The presence of these deeper trap levels was further substantiated and quantified by DLTS measurements in the same work.[62] Campbell *et al.*'s measurement showed the presence of deep, p-type majority bulk-traps that are distributed in energy.[62] Through temperature dependent measurements and extensive model fitting, the authors deduced a discrete trap level with an activation energy of *ca.* 750 meV above the HOMO and a concentration of *ca.* 5×10^{17} cm^{-3}. This readily supports the notion from the CV data that a large concentration of states is present deeper in the mid-gap of pure PPV films.

Indeed, a similar deep defect band in pure P3HT was predicted, not only by the TSC measurements in Section 3.1 (Fig. 3), but also by ultraviolet and inverse photoemission spectroscopy.[65] The photoemission spectra of Fig. 7 show a weak feature (labeled 'def') that cannot be associated with either molecular orbital.[65] This distribution occurs within the polymer bandgap and likely represents deep states. To gain further insights and quantification of the suspected band, we turn to capacitance *versus* frequency (CF) measurements (refer to Appendix section 8.5 for details).[39] Such measurements have directly revealed a Gaussian shaped deep trap band in neat P3HT diodes with $E_T = 390$ meV above the HOMO, $\sigma_T = 56$ meV and $N_T = 2.1 \times 10^{16}$ cm^{-3}.[39] One notes these parameters are somewhat different than those derived for PPV diodes but, nonetheless, illustrate a similar qualitative depiction. CV

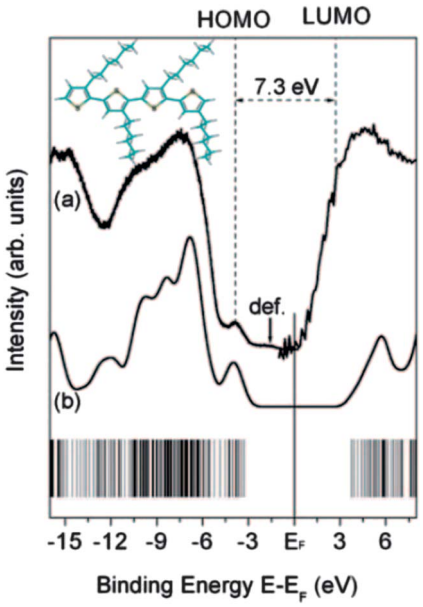

Fig. 7 Occupied (left) and unoccupied (right) molecular orbital contributions of regioregular P3HT to the (a) photoemission and inverse photoemission spectra, respectively, are compared with (b) theory. The experimental HOMO–LUMO gap of P3HT (7.3 eV) is indicated as is a defect state (def.) not directly attributable to the molecular orbitals indicated (see text). The inset shows a schematic of a single chain of regioregular P3HT. Reprinted with full permission from ref. 65. Copyright [2007], John Wiley and Sons.

measurements included with the cited CF experiment yield a ionized acceptor density of 3.2×10^{16} cm^{-3},[39] in line with that of Dennler's CV measured 5×10^{16} cm^{-3} for neat P3HT diodes.[13] Interestingly, if one considers the lower measurement frequency employed in Dennler's CV work (1 kHz) as well as the CF theory outlined in Appendix section 8.5, the known deep trap may be fully responding throughout the CV measurement. If we subtract the deep-band concentration (2.1×10^{16} cm^{-3})[39] from the measured N_A^- (5×10^{16} cm^{-3}),[13] a *real* ionized acceptor concentration of 2.9×10^{16} cm^{-3} is revealed. This is in excellent agreement with the aforementioned 3.2×10^{16} cm^{-3} and gives nice substantiation of the applied theory. Moreover, this highlights that $N_T \approx N_A^-$, indicating a substantial impact of N_T on the electronic properties, and thereby, photovoltaic performance should be expected.

As such, modeling techniques employing similar trap distributions should well describe the current characteristics of these OPV systems. In general, charge transport in a typical organic material is described by a hopping behavior. These current characteristics are usually explained with space-charge limited (SCL) and trap limited (TL) models. From this modeling, features of the dominate trap sites and their effects on charge transport can be readily studied (refer to Appendix section 8.3 for details). Nikitenko *et al.* have done just that with neat P3HT diodes.[56] In accordance with their TSC data (Fig. 3), a multiple trap formalism was employed with the assumption that a superposition of two Gaussian distributions makes up the energetic DOS.[56]

$$g(E) = \sqrt{\frac{2}{\pi}}\frac{(N - N_T)}{\sigma}\exp\left(-\frac{E^2}{2\sigma^2}\right) + \frac{N_T}{\sqrt{2\pi}\sigma_T}\exp\left(-\frac{(E - E_T)^2}{2{\sigma_T}^2}\right) \quad (1)$$

Numerical calculations coupled with this dual Gaussian were presented to study the model's general behavior. As expected, the simulations showed high voltages or a zero trap concentration induced currents close to the trap-free law (eqn (13) with $\theta = 1$), while variations of the N_T, E_T and σ_T parameters showed slope changes and voltages shifts in the current characteristics at intermittent biases.[56] Confident in its validity, the model was then applied to P3HT diode currents.[56] The experimental data was well explained by the defined model and the parameters summarized in Table 1.[56] As seen, this data supports the depicted shallow-deep tDOS and further quantifies their deep-trap band concentration at 1.5×10^{16} cm^{-3}. The trap density (N_T) as well as spreading parameter (σ_T) are in good agreement with the CF based work – though, the activation energy is somewhat higher. Nonetheless, this highlights these trap states have a controlling effect on charge transport.

Evidently, deeper distributions are present in neat donor materials. In both P3HT and PPV these deep traps have been identified and characterized. In P3HT a Gaussian distribution has been indicated, while in PPV a dominant discrete level. In both, a relatively high density of traps has been reported – $\geq 1 \times 10^{16}$ cm^{-3} – which is of the same order and, in some cases, even greater there than the density of relatively shallow states. Of course, thus far we have focused only on trap levels between the HOMO and mid-gap of these neat materials, however, we must also consider traps in the upper half of the gap.

3.2.3. Electron traps. The discussion on electron traps in donor materials is relatively straight forward as a recent work by Nicolai *et al.* unifies the presence of these deep states in popular OPV materials.[66] The authors leveraged a numerical drift-diffusion model coupled with a Gaussian distribution of states to study the current characteristics of electron-only organic diodes. Remarkably, the electron trap band was found to be fairly consistent with $E_T \approx -3.6$ eV below the vacuum level, $N_T \approx 3 \times 10^{17}$ cm^{-3} and $\sigma_T \approx 100$ meV for all tested materials.[66] In P3HT, for example, this corresponds to a trap depth of *ca.* 600 meV below the LUMO. One also notes the relatively high density of defects states. Thereby, piecing together the works discussed insofar to depict the complete trap profile between donor HOMO and LUMO, the cartoon of Fig. 1 is readily obtained – that is, Gaussian shaped molecular orbitals that decay into distributions of energetically shallow and deep trap states.

Table 1 Summary of important fitting parameters in Nikitenko *et al.*'s dual Gaussian SCL current work

	E (meV)	N (cm^{-3})	σ (meV)
Shallow band	—	1.0×10^{18}	55
Deep band	500	1.5×10^{16}	80

Interestingly, Nicolai *et al.*'s work implies that materials with an electron affinity approaching or larger than *ca.* −3.6 eV should exhibit trap-free electronic properties. Indeed, this was found true for both $PC_{60}BM$ (LUMO ≈ −3.9 eV) and poly[{*N*,*N*′-bis(2-octyldodecyl)-naphthalene-1,4,5,8-bis(dicarboximide)-2,6-diyl}-*alt*-5,5′-(2,2′-bithiophene)] (P(NDI2OD-T2); LUMO ≈ −4.0 eV), both of which gave trap-free SCL electron transport.[66] Of particular interest is the former, which is a commonly used acceptor in today's OPV cells. Having established a more detailed view of the electronic traps in neat donor materials, we now turn our attention to the other half of the blend: acceptor materials.

3.3. Levels in acceptor materials

As discussed in Section 1, most modern day OPV devices comprise both donor and acceptor materials. Neat donors have been discussed thus far; let us now visit the latter. Methanofullerenes are commonly employed acceptors and may contain bandgap residing trap states. Though $PC_{60}BM$ was shown to exhibit trap-free electron transport,[66] others have indicated electron trapping in acceptor materials, especially the higher adduct fullerenes.[67] As an example of directly identifying such states, the conventional and T_{start}–T_{stop} TSC measurements were again applied.[68] Bis[6,6]-phenyl-C61-butyric acid methyl ester ($bisPC_{61}BM$), [6,6]-phenyl-C71-butyric acid methyl ester ($PC_{71}BM$), and $PC_{61}BM$ based devices (ITO/PEDOT:PSS/PCBM/lithium fluoride (LiF)/Al) were studied. Fig. 8 shows the

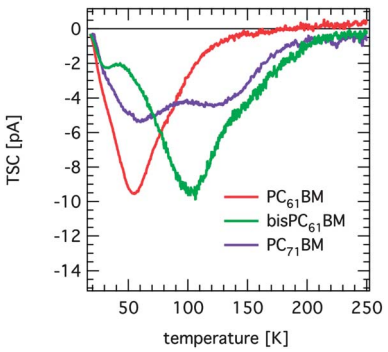

Fig. 8 TSC spectra of $PC_{61}BM$, $bisPC_{61}BM$ and $PC_{71}BM$. Reprinted with full permission from ref. 68. Copyright [2011], John Wiley and Sons.

Table 2 Lower limit of the trap densities of $PC_{61}BM$, $BisPC_{61}BM$ and $PC_{71}BM$, as well as the temperatures of the TSC maxima and the corresponding activation energies estimated by the T_{max} method according to eqn (4). For $bisPC_{61}BM$ and $PC_{71}BM$ E_t and T_{max} values of both peaks are shown. Reprinted with full permission from ref. 68. Copyright [2011], John Wiley and Sons

Sample	Trap density [m^{-3}]	T_{max} [K]	E_t [meV]
$PC_{61}BM$	$\geq 1.7 \times 10^{22}$	54.9	86
$bisPC_{61}BM$	$\geq 2.3 \times 10^{22}$	32.4	45
		103	184
$PC_{71}BM$	$\geq 2.0 \times 10^{22}$	60.1	96
		121.4	223

resulting [conventional TSC] spectra, whose quantification is summarized by Table 2.[68]

Interestingly, all three materials showed at least one distinct trap distribution, with bis$PC_{61}BM$ and $PC_{71}BM$ showing the presence of a second, deeper level. Each methanofullerene exhibited a markedly different TSC spectrum. A common feature was noted between $PC_{61}BM$ and bis$PC_{61}BM$, where a low temperature peak in bis$PC_{61}BM$ (*ca.* 32 K or 45 meV) closely matched a slight $PC_{61}BM$ TSC shoulder (Fig. 8) – signifying a common defect level.[68] To give some substantiation, DLTS measurements on neat $PC_{61}BM$ films (ITO/PEDOT:PSS/$PC_{61}BM$/LiF/Al) also showed a single shallow trap band in this range, however, with a somewhat lower activation energy (21 meV).[58] At first sight this shallow $PC_{61}BM$ level seems to be in contrast to the trap-free electron transport discussed earlier.[66] However, this can be reconciled by considering the trap band magnitude. It is well know that for a Gaussian distribution of *shallow* traps, the space charge limited current is approximated by a modified Mott–Gurney law (see eqn (13)). A quadratic current–voltage relationship coupled with a reduced [effective] mobility is then exhibited. The effective mobility is given by $\mu_p\theta$ and,

$$\theta = \frac{\langle n_c \rangle}{\langle n_c \rangle + \langle n_t \rangle} \quad (2)$$

where $\langle n_c \rangle$ is the average free carrier concentration throughout the thickness and $\langle n_t \rangle$ the average trapped charge. As previously stated, the trap-free case has $\theta = 1$. The free carrier concentration in $PC_{61}BM$ is in the range of 1×10^{18} cm^{-3} and, for a conservative estimate, consider the trapped charge to be in the range 1–2 $\times$ 10^{16} cm^{-3}. This gives a θ approaching 1 and indicates trap-free electron transport should be expected. Nonetheless, the TSC of all three materials indicated a continuous distribution of trap states throughout the measured energy regime. This point is confirmed by fractional TSC measurements on $PC_{61}BM$, which further quantified the tDOS.[68] When comparing these three commonly employed materials, both bis$PC_{61}BM$ and $PC_{71}BM$ showed further broadening in the TSC signal and slightly higher trap concentrations with significantly deeper energies.[68] This indicates a higher amount of energetic disorder and electron trapping in these two derivatives and explains lowered dark currents through these materials.[68]

This TSC work supports the general depiction of the neat acceptor tDOS presented in Section 3.1 and further quantifies the states present in common acceptors. Clearly, the pure acceptor materials of OPV devices are subject to energetic disorder and bandgap residing trap level. The impact of these states on photovoltaic performance will be revisited in Section 4.3. Next, trap origins in these neat materials are discussed.

3.4. Trap origins: oxygen, structural and synthesis residuals

To give some idea as to the sources of the trap levels discussed above, this section explores studies centered on defect level origins in neat OPV materials. Both extrinsic and intrinsic sources are considered, namely: oxygen/moisture, structural disorder and synthesis residuals.

As mentioned throughout the article and hinted at by the aforementioned CV work,[13] oxygen and moisture have been identified as key sources of p-type doping in donor materials. This indicates these extrinsic impurities generate or alter bandgap residing levels of interest. To begin this discussion, we return to the P3HT TSC work presented by Schafferhans *et al.* (Fig. 4).[57] In the report, the conventional TSC measurement was repeated as a function of both air and pure oxygen exposure. After 96 h of O_2 treatment, the magnitude of the 105 meV band nearly tripled, while the 50 meV remained unchanged.[57] Similar effects were noted for air exposure. This shows that the shallower, 50 meV band is likely intrinsic (structural) in nature. Though, other chemical impurities cannot yet be ruled out. More notably, this shows the dominate 105 meV band is likely extrinsic in nature and heavily related to oxygen. Interestingly, photo-charge extraction by linearly increasing voltage (photo-CELIV) measurements show that after 100 h of air exposure, the mobility dropped by nearly 50$\times$. Clearly, oxygen plays a role in generating or, at the least, altering some portion of the shallow trap distribution in neat P3HT, and thereby, the electronic properties.

An earlier work on the interaction of oxygen with poly(3-alkylthiophenes) helps to further explain this oxygen related defect and the noted effects on carrier mobility.[9] Abdou *et al.* theorized a charge transfer complex (CTC) would form between oxygen and the polymer, with a lowest binding energy on the order of *ca.* 1.9 eV.[9] Further, it was thought that this CTC state might facilitate charge transfer and the formation of excess charge carriers, thereby affecting electronic properties. To detect this possible band, the group studied UV-vis absorption of P3HT films in the presence of oxygen and nitrogen (Fig. 9). As can be seen, nitrogen had essentially no effect on the measured optical density. In contrast, oxygen induced significant changes, especially near *ca.* 630 nm or 1.97 eV – strongly implicating the predicted CTC.[9] This complex formation is supported by the later work of Aguirre *et al.*, who have also extended this concept to another polymer.[48] Though the most substantial change in optical density occurred near 630 nm, it is clearly seen that oxygen induces changes throughout the sub-gap energies (Fig. 9). This introduces the idea that oxygen

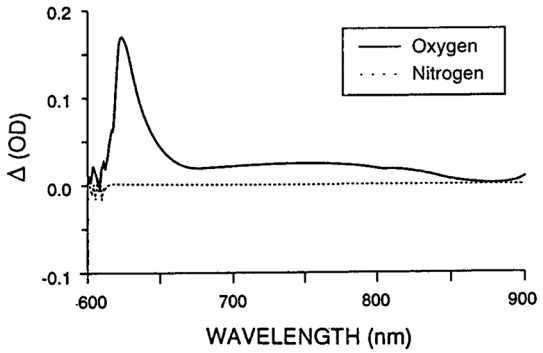

Fig. 9 UV-vis absorption spectra of a P3HT thin film (20 μm) in contact with oxygen (10 atm) and under oxygen-free N_2. Reference, O_2-free film. Reprinted with permission from ref. 9. Copyright [1997], American Chemical Society.

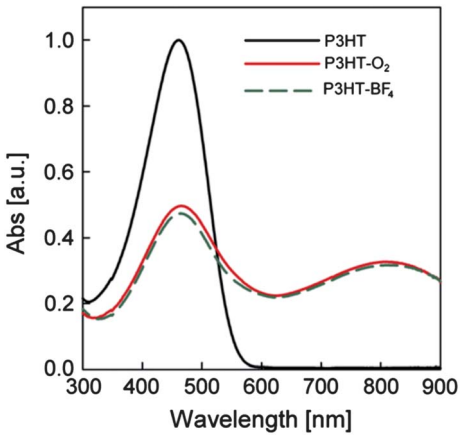

Fig. 10 Comparison of UV-vis spectra of P3HT in *o*-dichlorobenzene solution with the spectra of the P3HT solution after exposure to molecular oxygen ($P3HT^{+}$–O_2^{-}) and $NOBF_4$ (P3HT–BF_4^{-}). Reprinted from publication ref. 69, Copyright [2012], with permission from Elsevier.

in itself affects and/or generates a continuous distribution of levels throughout the bandgap. Such a thought is also supported by a recent UV-vis study on P3HT in solution form (Fig. 10).[69] Here, a broad sub-gap absorption band about *ca.* 810 nm was induced by oxidant treatments of molecular oxygen (O_2) as well as nitrosonium tetrafluoroborate ($NOBF_4$). Interestingly, the absorbance for wavelengths between *ca.* 300 and 550 nm was noticeably reduced. A similar decrease at moderate wavelengths coupled with an increase at longer wavelengths was also noted for treated polymer films, though not nearly as pronouced.[69] Intuitively, one might expect the noted changes to have effects on the electronic properties of these film.

To detect such changes, Abdou *et al.* measured the effects of oxygen pressure on both the conductivity and mobility of P3HT based field-effect transistors. In the presence of increasing oxygen pressure, conductivity was found to increase, while mobility was found to decrease.[9] An analogous case is well known for inorganic semiconductors with increasing doping concentrations.[52] This strongly indicates oxygen facilitates the presence of extra carriers and helps explain the degraded mobility noted by Schafferhans *et al.* during the exposure experiments.[57] The presence of these oxygen induce charge carriers has been more directly observed in the afore-discussed work of Dennler *et al.* (Fig. 5).[13] As mentioned, through successive CV measurements in open air, the group found the ionized acceptor density increased by a half order of magnitude (5.0×10^{16} to 1.0×10^{17} cm^{-3}).[13] This gives a quantification to Abdou *et al.*'s carrier concentration increase and further highlights the strong effect of oxygen/moisture on the shallow impurity states.

In like fashion, the electron traps noted by Nicolai *et al.* were also imputed [at least in part] to oxygen. As discussed, the electron-trap parameters between numerous materials were found to be similar. This indicates a common origin and rules out structural disorder. Through quantum-chemical calculations, the authors track down this origin and suspect hydrated oxygen complexes as the likely culprit.[66] Evidently, oxygen and moisture play a dominate role in the complete bandgap tDOS of acceptor materials.

Like donor materials, air and oxygen exposure have also been shown to have significant effects on the on the energetic tDOS of C_{60} and C_{70} films. In the case of C_{60}, exposure was found to greatly enhance the PDS spectrum of the deeper, localized states, while leaving the shallow-tail largely unaltered.[54] TSC experiments on C_{60} based transistors adds to this, pin-pointing a trap band center on *ca.* 230 meV that was greatly affected by exposure and an even deeper band centered on *ca.* 370 to 420 meV which remained unchanged.[15] This again depicts a defect distribution in which some bands are dominated by structural disorder, while others are heavily influence by oxygen and/or moisture. Of course, other extrinsic chemical impurities from material synthesis or device fabrication may contribute to the overall tDOS and are incidentally lumped in with the structural disorder here. As is the case with the donor materials, these oxygen induced modifications in C_{60} are also accompanied by a significant decrease in carrier mobility.[15,70,71] Contrarily, in the case of C_{70}, the sub-gap absorption coefficient was actually found to decrease with oxygen exposure, hinting that O_2 may be beneficial in terminating some inherent defects.[55] Interestingly, oxidant treatments (O_2 and $NOBF_4$) of PCBM in solution form did not produce any changes in the optical density.[69]

Defect origins from residuals left during material synthesis must also be considered. Though reports linking the contaminant impurities to specific trap-band energies could not be found, it is well-known that these synthesis residuals produce electronic-property altering states. Mentions to contaminates from starting reagents, nickel, copper and rhodium catalysts, *etc.* can be found.[17,72] However, maybe most prominent in the literature is residual palladium. A majority of conjugated polymers are synthesized *via* Stille or Suzuki coupling reactions – which are catalyzed by palladium complexes.[18,72] Residuals of this transition metal have been reported and linked to a degradation of electronic properties and photovoltaic performance.[17,18,72,73] In the case of PPV, residual palladium nanoparticles were found to induce shorts, greatly lowering the resistance of the film.[17] Even very small, hard to detect amounts (*e.g.* <0.1% by weight) of contaminate can have an effect on material properties and OPV performance.[17,18,72] The effects of residual catalysts on OPV performance will be subsequently revisited in Section 4.5.

Nonetheless, it is evident that commonly used, pure donor and acceptor OPV materials are trap-rich semiconductors with electronic properties closely tied to their intrinsic and extrinsic induced defects. A depiction of energetic disorder with multiple defect levels both shallow and deep has been given and elucidations as to the origins of these traps has been presented. We now move to a discussion on how this defect profile changes in the popular BHJ OPV structure; comprising bulk blends of the donor and acceptor materials discussed above. The sources of these defects will be revisited and the effects of these defects of BHJ photovoltaic conversion will be examined.

4. Identification and characterization: blended material systems

4.1. General depiction

Having examined neat films, it is a logical step to now look at the tDOS of the blended systems which make up modern day OPVs. First, the PDS data of Goris *et al.* should be revisted.[53] As seen in Fig. 2, when compared to neat materials, the spectra of blended devices showed a more intricate distribution which extended deeper into the gap.[53] This strongly indicates a higher degree of disorder in both PPV:PCBM and P3HT:PCBM BHJ devices. This story of stronger disorder was recently corroborated and further resolved by Neugebauer *et al.*, who have leveraged DLTS measurements to compare the trap bands of neat P3HT and PCBM to that of blended films.[58] The activation energies and relative trap concentrations are shown in Fig. 11. As can be seen, a comparison to TSC measurements on neat P3HT,[57] neat PCBM[68] and a blend thereof[37] has also been included. One recalls that the neat-film DLTS data has been already mentioned and both materials showed a single, dominate trap level with an activation energy of 21 meV for PCBM and 87 meV for P3HT.[58] The DLTS of blended films, however, presented with numerous emission spectra, indicating multiple trap-levels throughout the tDOS. At the low end of the energy spectrum, a trap 'A' with an activation near 28 meV was found. This corresponds reasonably well to the DLTS measured trap in neat $PC_{60}BM$ (21 meV), indicating its contribution to blend tDOS.[58] The most concentrated band 'E' has an activation energy of *ca.* 100 meV and correlates well the TSC (105 meV) measured neat P3HT trap,[57,58] potentially indicating the polymer's contribution. The other bands, 'B–D' and 'F', are unique to the blended system. This readily supports the general depiction of greater energetic disorder upon mixing the neat materials and highlights the presence of more charge traps in these BHJ devices. Let us now further detail and quantify this added disorder.

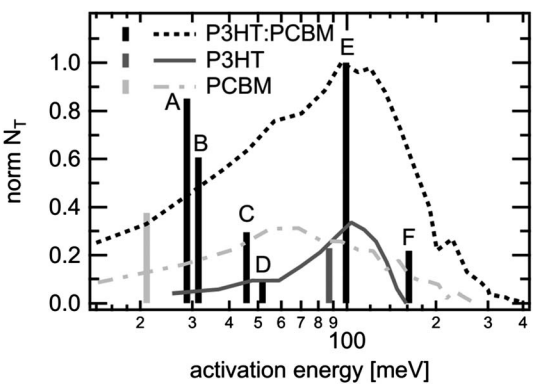

Fig. 11 Bars: overview of the obtained activation energies in PCBM (light grey), P3HT (dark grey) and P3HT:PCBM blend (black) and relative maximum N_T in the spectrum found by I-DLTS. Lines: normalize activation energy spectra of earlier TSC measurements[37,57,68] (colors are as above). Reprinted with permission from ref. 58. Copyright [2012], American Institute of Physics.

4.2. Levels in the donor and acceptor portions and blend unique bands

As referenced in Fig. 11, trap bands in blended devices have also been examined through TSC measurements.[37] An ITO/PEDOT:PSS/P3HT:PCBM/Ca/Al structure was studied. Three TSC bands were found. Two (50 and 105 meV) precisely matched the bands of their earlier neat P3HT TSC work,[57] while the third, which was centered deeper in the gap at 250 meV, was unique to the blend.[37] When comparing the TSC spectrum in blended devices to that of the neat films, a substantial broadening and increase in concentration was also seen.[37,57] This, coupled with the existence of the unique, deeper band in the BHJ devices, again shows higher energetic disorder in blended systems. It is immediately clear that the dominate band centered at *ca.* 100 meV is common between the DLTS and TSC blended film work.[37,58] Interestingly, the TSC 50 meV band, which the authors attributed to a polymer contribution, correlates well with DLTS bands 'C' and 'D', which were considered unique to the blend in the DLTS experiment.[37,58] Neglecting the disagreement in origin, DLTS bands 'C–D' seem to give more resolution to the TSC 50 meV, indicating two, closely spaced and overlapping trap sites make up this energy regime. The TSC 250 meV is in qualitative agreement with the DLTS 'F' band (*i.e.* both unique and somewhat deeper levels), albeit with a *ca.* 90 meV larger activation energy. The total trap density in the measured regime was estimated at 8×10^{16} cm^{-3} – 8× higher than that measured for neat P3HT, 4× higher than that of neat $PC_{60}BM$ and nearly 3× higher their simple addition (P3HT + $PC_{60}BM$).[37,57,68]

In 2012, Yu *et al.* also weigh in on the trap distribution of P3HT:PCBM blended films.[74] The authors studied both conventional and T_{start}–T_{stop} TSC measurements on ITO/P3HT:PCBM/Al structured cells.[74] Conventional TSC revealed two trap bands, centered on 140 and 220 meV, not unlike the DLTS (160 meV) and TSC (250 meV) bands, respectively.[37,58,74] The group hypothesized more bands existed in this energy range, but were unresolved by the conventional TSC measurement. Thus, they turned to fractional TSC along with an extensive numerical fitting to further resolve a complete picture of the tDOS. In all, five levels were cited (Table 3). As noted, both exponential and Gaussian distributions were seen with concentrations ranging between 8.0×10^{16} and 1.5×10^{19}

Table 3 Parameters of electrically active trap distributions used in the curve-fitting procedure. Reprinted from publication ref. 74, Copyright [2012], with permission from Elsevier

		Distribution				
			Gaussian		Exponential	
	E_a (eV)	Type	N_{g0} (cm^{-3})	σ (meV)	N_{t0} (cm^{-3})	E_t (eV)
N_1	0.06	Exp.	—	—	1.8×10^{17}	0.03
N_2	0.12	Exp.	—	—	2.5×10^{18}	0.03
N_3	0.14	Gauss.	8.2×10^{16}	52	—	—
N_4	0.20	Exp.	—	—	1.5×10^{19}	0.03
N_5	0.35	Gauss.	2.7×10^{18}	48	—	—

cm^{-3}, significantly larger than that found in Schafferhans's bands. Again, two bands (N_3 and N_4) are in qualitative agreement with the DLTS 'F' (160 meV) trap and TSC 250 meV levels, respectively. Interestingly, the newly resolved N_2 is somewhat similar to the dominate 'E' band of Fig. 11, while N_1 can be likened to the 'C–D' distribution. The authors theorized that traps N_1–N_3 stemmed from properties of the neat P3HT, while N_4 might have resulted from the addition of PCBM – somewhat different than the previous TSC and DLTS interpretations. Maybe most interesting is the deeper N_5 trap state. This band is only vaguely seen in other TSC data, but showed a strong presence here. According to the authors, this type of level is often observed at the high-temperature edge and may be due to a weakening of the stimulated current.[74] However, a similar band has also been noted through other techniques, potentially substantiating its existence. Further, one recalls the existence of a similar deep band in neat donor materials (Section 3.2.2). Let us now turn attention to this band.

Prior to Yu's work, this deep band had been studied using both CF and current modeling methods.[39,75] The first such work came in 2009 and centered on an ITO/POEDOT:PSS/P3HT:PCBM/Ca/Ag structure. The CV work of Dennler *et al.* had shown the existence of a Schottky junction between the organic and metal cathode.[13] Similar behavior was then suggested for blended films, allowing capacitance techniques to be leveraged on a BHJ system.[76,77] Employing the CF measurement (refer to Appendix section 8.5 for details), Boix *et al.* revealed a prominent, Gaussian shaped deep defect band centered at *ca.* 380 meV above the HOMO, with $N_T = 1.2 \times 10^{16}$ cm^{-3} and $\sigma_T = 66$ meV (Fig. 12), very similar to that mentioned in neat donor films.[39] For reference, an attempt to escape frequency (ν_0) of 1×10^{12} s^{-1} was used (see eqn (19)). One notes the immediate proximity of this band to the FTSC N_5 trap (albeit two orders of magnitude lower in density),[74] giving support to the presence of this deep trap in blended systems. Further, by comparing the energetic profile for active layers comprising different P3HT:PCBM loadings – namely, 1 : 0.0, 1 : 0.4, 1 : 0.6, 1 : 0.8, 1 : 1.2 and 0 : 1.0 – Boix *et al.* showed the measured deep-defect distribution is not significantly affected by the presence of PCBM. This indicates that the band is inherent to the polymer donor. Interestingly, CV measurements show the ionized acceptor density in the blended films (*ca.* 4.3×10^{16} cm^{-3}) is only slightly larger than that of neat P3HT devices (3.2×10^{16} cm^{-3}).[39] This indicates that the higher energetic disorder in blended films may not have a large effect on carrier concentration in these already moderately doped films.

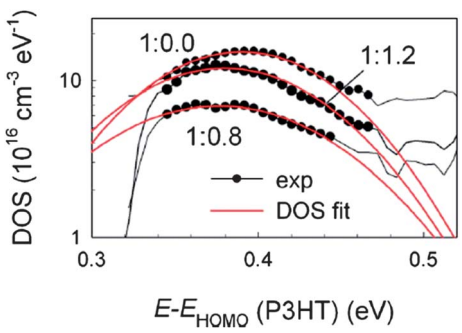

Fig. 12 Density of defect states as a function of the energy with respect to the P3HT HOMO level (demarcation energy), $E - E_{HOMO}$, calculated using eqn (3) [of the original article] and the capacitance spectra in Fig. 1(a) [see original article]. Gaussian DOS fits (eqn (5) [see original article]) are also displayed. Composition of the blend is marked in each distribution. Reprinted with permission from ref. 39. Copyright [2009], American Institute of Physics.

It is worth noting, Boix *et al.* later revised the mean energy of this defect band, citing a newly revealed attempt-to-escape frequency of 33.42 s^{-1} *via* temperature dependent CF measurements.[78] This gives a revised mean energy of *ca.* 35 meV – an order of magnitude lower than the previously reported value and more like the DLTS 'A–B' bands than the TSC N_5 band.[78] For some comparison, similar temperature dependent CF measurements have also been conducted on ITO/MDMO-PPV:PCBM/Al[79] and ITO/PEDOT:PSS/MDMO-PPV:PCBM/Al[80] based devices. The former finds a shallower trap centered on 24 to 34 meV with a ν_0 in the range of 1×10^7 s^{-1} (estimated from presented data).[79] The latter report finds two trap bands centered on 9 meV and 177 meV with characteristic escape frequencies of 1.3×10^7 s^{-1} and 7.6×10^9 s^{-1} respectively.[80] Campbell *et al.* also found an attempt-to-escape frequency in this range (1×10^8 s^{-1}) for PPV based devices, further corroborating the characteristic prefactor.[62] One notes the sharp difference in ν_0 between the P3HT and PPV materials and, of course, this highlights the necessity of obtaining an accurate value if one is to properly interpret measurements relying on emission data. It is also worth highlighting that Dyakonov *et al.*'s temperature dependent CF data shows similar trap behavior in PPV:$PC_{60}BM$ blended films to that in P3HT:$PC_{60}BM$ devices. From shallowest to deepest, bands with activation energies at 9, 22–34 and 177 meV have been identified and, of course, we might expect the presence of a the deeper, 750 meV level revealed by Campbell[62] in neat PPV – showing the qualitative resemblance to Fig. 11.

Nonetheless, the N_5 trap band in P3HT:$PC_{60}BM$ BHJ devices was also shown by Nam *et al.* through current modeling measurements.[75] The authors used SCL and Poole–Frenkel current models to study trap band concentrations in air-processed ITO/PEDOT:PSS/P3HT:PCBM/gold (Au) OPVs.[75] The selective Au cathode allowed hole transport (in the donor) to be isolated in reverse bias, which was subsequently subtracted from forward bias characteristics to yield information on the electron transport (in the acceptor). Hole current through P3HT was described by three main regions: (i) trap-filled SCL current in lower voltages, (ii) Poole conduction in intermediate voltages and (iii) Fowler–Nordheim tunneling at higher voltages. From region (ii), the total concentration of mid-gap states in the donor was calculated to be *ca.* 6×10^{20} cm^{-3}.[75] This value is two to four orders of magnitude higher than what is typically reported for neat or blended cells. However, these devices were processed in open air, which is known to increase the impurity concentrations. The effects of oxygen on trap states in blended systems will be more directly addressed in Section 4.5. In any case, at the intersection of regions (i) and (ii), the average trap activation energy was calculated in the range of 300 to 500 meV

– in agreement with the TSC measurements and unrevised CF work deep defect band.[39,74,75] As an interesting note, as expected from the neat film discussion, hole mobility in these air-processed devices was substantially lower than the typical values for devices processed in more inert atmospheres.

Continuing with Nam's work, electron transport in the $PC_{60}BM$ was also described by three main regions: (i) Schottky limited at lower bias, (ii) power-law SCL current at moderate bias and (iii) trap-free SCL current with a field-dependent mobility at higher biases. Using region (ii), with the assumption of an exponential DOS and the eqn (11) simplification (refer to Appendix section 8.3 for details), the authors found a relatively high electron trap density of *ca.* 1×10^{18} cm^{-3}.[75] As with the case of hole traps, they suspect this heightened density to be oxygen-related stemming from the open air fabrication – a thought which is supported by the afore-discussed optical works centered on C_{60}, oxygen exposure and sub-gap states.[54,55] Interestingly, a blend-annealing process greatly increased the degraded electron mobility and pushed the power-law electron conduction towards trap-free transport.[75] This aligns their PCBM electron transport with that reported by Nicolai *et al.* for inert atmosphere processed diodes and indicates that significant traps in $PC_{60}BM$ (and other acceptors) may be present if oxygen exposure is appreciable.[66] Further, this highlights the well-known fact that thermal annealing is effective at removing structural defects and introduces the idea that oxygen induced states may be revisable by thermal treatments. This point is built upon in Section 6.

In blends comprising of higher adduct fullerenes (*e.g.* $bisPC_{61}BM$), enhanced disorder and electron trapping [when compared to $PC_{60}BM$ based blends] has been reported.[67] Lenes *et al.* investigated such solar cells and found a sharp reduction in the current–voltage characteristics of electron single-carrier devices. Coupled with a Gaussian disorder model, enhanced energetic trapping in the higher adducts was found – in-line with that expected from the TSC measurements on neat fullerene films as discussed in Section 3.3.[67,68] Interestingly, the authors found that this additional disorder did not have any detrimental effects on the photovoltaic performance of the blends – indicating these traps are rapidly filled under illumination.[67] This leads nicely into a discussion on how defects affect OPV performance. Clearly, trap states should only be considered if they have a substantial impact on electronic properties and photovoltaic conversion. The subsequent section discusses some important works highlighting such impacts.

4.3. Traps and OPV performance

Continuing the dialog on the impact of disorder in the acceptor portion, others have indicated these states may indeed have adverse effects on the achievable performance, even in $PC_{60}BM$ based BHJ devices. Garcia-Belmonte *et al.* have investigated the effects of fullerene electronic states in blended devices through open-circuit impedance spectroscopy (IS) (refer to Appendix section 8.7 for details).[35] In the cited work, BHJ cells derived from blends of P3HT and $PC_{60}BM$ were compared to that of blends of P3HT and 4,4′-dihexyloxydiphenylmethano[60] fullerene (DPM_6).[35] A significant positive shift in the V_{oc} of the DPM_6 device was noted.[35] To study its origins, the open-circuit impedance was measured at Illumination intensities corresponding to a V_{oc} between *ca.* 200 and 800 mV. An energetic DOS was then generated, where $g(E_{Fn})$ was taken to be a single Gaussian distribution (Fig. 13).[35] The displayed states were termed *intermediate* to signify they lay below the fullerenes' upper lying LUMO,[35] indicating the measured DOS may be a part of the LUMO tail or a separate band altogether. Clearly seen in Fig. 13 is a slight shift in central energy and a significant increase in the concentration of the $PC_{60}BM$ intermediate states. As a result, it is concluded that E_{Fn} in PCBM based devices is *pinned* at deeper energies within the intermediate-DOS distribution. This induced a reduction of the difference between the polymer E_{Fp} and fullerene E_{Fn}, thereby, reducing the achievable V_{oc}.

Further, such bandgap residing states in both donor and acceptor portions of OPV devices may be detrimental to photovoltaic performance through recombination enhancement, especially if they are spatially located at or near a donor–acceptor domain interface. A recent work by Street *et al.* highlighted this by systematically exploring the recombination kinetics in BHJ organic solar cells, carefully examining the possibility of Auger, geminate and non-geminate exciton and interface state recombination. Though a series light-intensity and temperature dependent experiments coupled with theoretical modeling, the authors suggested mono-molecular recombination through defects occurring at or near the domain interface(s) as a dominant loss mechanism plaguing photovoltaic performance.[32] It should be stated that these experiments were conducted on PCDTBT (poly[[9-(1-octylnonyl)-9*H*-carbazole-2,7-diyl]-2,5-thiophenediyl-2,1,3-benzothiadiazole-4,7-diyl-2,5-thiophenediyl]) $PC_{70}BM$ BHJ devices, however, the authors feel the conclusions may be general to other blended systems

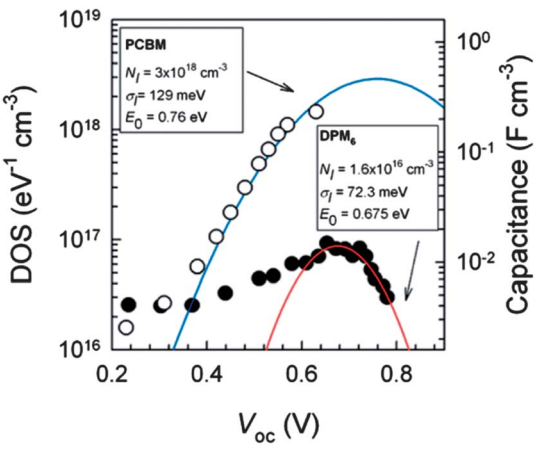

Fig. 13 Capacitance values extracted from fits of the low-frequency arc of the impedance spectra as a function of V_{oc} reached under varying illumination levels. White dots correspond to PCBM-based solar cells and black dots to DPM_6-based solar cells. Gaussian DOS (solid lines) and distribution parameters resulting from fits. Reprinted with permission from ref. 35. Copyright [2010], American Chemical Society.

(such as P3HT:PCBM).[32] Street *et al.* have also given some guidance as to improving OPV conversion efficiency – intuitively, by reducing the density of states at or near the domain interfaces. Interestingly, given a thicker device (200 nm), the model employed by Street *et al.* suggested that even an order of magnitude reduction of the interface states could as much as double the device's photovoltaic conversion efficiency.[32] It is worth noting that some disagreement on this topic can be found throughout the literature.[81,82]

Other works have investigate trap-assisted recombination more emperically.[31,33] Cowan *et al.* studied such a case for PCDTBT:$PC_{60}BM$ devices.[33] The introduction of $PC_{84}BM$ impurities to the blend induced dramatic losses in the photovoltaic performance of the devices. Impurity concentrations as low as one part in one thousand were found to reduce conversion efficiency.[33] The losses were directly linked to the intentional addition of theses electronic states, which augmented trap-assisted recombination, hampered charge transport and reduced carrier mobility.[33] By monitoring the open circuit voltage as a function of light intensity and trap density, the authors also gave some indication as to the impurity-level threshold where trap-assisted losses become significant. This threshold will be contingent on several factors – with the trap density and generation rate (light intensity) being the most notable.[33] Qualitatively speaking, Cowan *et al.* propose trap-assisted recombination effects become dominant at high trap densities and/or low light intensities. The works of Mandoc *et al.* give some substantiation.[31,83] In the first, the authors investigated the deliberate introduction of electron traps to devices derived from blends of PPV and $PC_{60}BM$.[31] A degradation of open circuit voltage, short circuit current and fill factor was clearly seen. Again, the losses were attributed to an enhancement in trap-assisted recombination,[31] highlighting in the limit of high trap densities, trap-assisted losses can dominate. In a second work, Mandoc *et al.* studied all polymer solar cells based on a blend of PPV and PCNEPV (poly-[oxa-1,4-phenylene-(1-cyano-1,2-vinylene)-(2-methoxy-5-(3′, 7′-dimethyloctyloxy)-1,4-phenylene)-1,2-(2-cyanovinylene)-1,4-phenylene]).[83] No extra traps were added, however, inherent electron traps in the acceptor portion gave rise to a dominant trap-assisted recombination loss, but only at low light intensity.[83] This gives substantiation to the second portion of Cowan *et al.*'s proposal. This also shows that in current and new material systems variations in structural disorder (inherent to the material or by varying fabrication parameters), variations in oxygen exposure, variations in synthesis impurities, *etc.* may induce varying amounts of trap-assisted losses – indicating trap states should be carefully monitored. Further, even if the trap states are kept at a reasonable level, they should not be forgotten as these solar cells under normal operating conditions will see lower light intensities, and thereby, trap-assisted loses.

Aside from trap-assisted recombination, charge trapping is also thought to facilitate space charge effects.[34,84] In a 2009 report, Mcneill *et al.* studied photocurrent transients in all polymer BHJ cells to reveal the trapping and detrapping of electrons.[34] The transients were induced by the application of a square light wave at a given frequency, of which the pulse width, intensity and presence of background illumination (also of varying intensity) were varried.[34] A sharp transient peak just after *turn on* of the pulse coupled with long transient tail after *turn off* was revealed and attributed to the trapping/detrapping of electrons. The authors proposed such trapping may facilitate space charge effects, where charges trapped near the anode would perturb the internal electric field to: (i) decrease the probability of charge separation and (ii) promote bimolecular recombination.[34] Both of which yield loses in conversion efficiency.

Before continuing on to a discussion on trap origins, it is worth segwaying to the identification and characterization of electronic defects at the edges of the blend; that is, at the blend–electrode interfaces.

4.4. Electrode interface states

Electronic states at the interfaces between the BHJ blend and charge collection layers have also been identified. Towards the anode, Ecker *et al.* have profiled trap bands using the CF measurement in ITO\hole transport layer (HTL)\P3HT:PCBM\Ca\Al structured cells.[85] Devices comprising different HTLs, namely PEDOT:PSS and polyaniline:poly(styrene sulfonate) (PANI:PSS) based in water and alcohol solvents, were examined.[85] The CF experiments were conducted under 16 mW cm^{-2} and 100 mW cm^{-2} illuminations at open circuit conditions. Two Gaussian distributions in the energetic tDOS were revealed. The first, lower energy distribution was attributed to bulk states. A ν_0 was not measured or assumed, thus, a comparison with the other CF experiments cannot be made. Though, it is likely that these states are the same deep states as those previously mentioned.[22,39] The second, higher energy Gaussian was attributed to electronic states at the HTL interface. The concentration of the interface states was found to be significantly higher than that of the bulk states, highlighting their strong presence in this system. Interestingly, non-encapsulated devices with HTLs based in water solvents presented with additional trap states at the blend–HTL interface,[85] showing the importance of defect considerations when choosing such interlayers. It is interesting to speculate how these traps may affect OPV performance. Most conducive may be the space charge effects discussed by McNeill *et al.*, where charges trapped near the anode may retard charge separation and promote bimolecular recombination.[34]

Near the cathode, Bisquert *et al.* have also identified interface trap states.[86] Similar to Ecker *et al.*, the interface states were identified through capacitance measurements under illumination – here, CV measurements on an ITO/PEDOT:PSS/P3HT:PCBM/Al structure was studied.[86] The extracted ionized acceptor density was similar in both dark and illuminated conditions (*ca.* 4–5.0 $\times$ 10^{16} cm^{-3}); however, the built-in potential was found negatively shifted by 0.6 V in the illuminated case. This shift is explained through a photovoltaic model which incorporated a concentration of kinetically slow surface states at the organic–metal junction.[86] Under illumination an accumulation of minority charges, and thereby a charging of surface states, induces band unpinning and the noted V_{bi} shift.[86] This change in energetics may significantly alter

photovoltaic performance,[86] again highlighting the importance of defect considerations at layer interfaces. Further quantification of these states has not yet been given.

4.5. Trap origins: oxygen, structural and synthesis residuals

Having discussed the identification of trap states throughout the BHJ structure, let us now find some indication as the origins of the blend-film trap states. We first return to the 2010 TSC work on BHJ ITO/PEDOT:PSS/P3HT:PCBM/Ca/Al structures.[37] Coupled with the thermal experiments, CELIV and IV measurements as a function of synthetic air (80% N_2, 20% O_2, <1 ppm H_2O) exposure were examined. Upon exposure, in contrast to the case of neat P3HT, the magnitude of the 105 meV trap appears to decrease.[37,57] However, a new band at *ca.* 142 meV emerged, with a concentration linked to exposure time.[37] As a result, the total trap density in the measured energy spectrum remained constant through 100 h of exposure.[37] Though, it must be noted that the measurement only gives a lower limit for the total trap density (refer to Appendix section 8.1 for details). The recombination of charge carriers could be masking an increase in trap density and/or causing the apparent decrease of the 105 meV band. Nonetheless, it is clear that oxygen is inducing or augmenting states somewhat deeper in energy. This data is supplemented with CELIV mobility and carrier density measurements. A decrease in carrier mobility along with an increases in charge density was found.[37] This is in line with that expected from the discussion on unblended systems. This data, coupled with macroscopic simulations, is correlated to degradations in the solar cell IV. The authors assert increased carrier densities dominate the degradation of J_{sc}, while the increased deep(er) trap concentration may be at the origin of V_{oc} and FF degradation,[37] perhaps through enhanced trap-assisted recombination losses and space charge effects. The link between excess charge carriers and J_{sc} degradation is supported by Seemann *et al.*, who noted a large portion of oxygen-induced degradation stems from excess mobile holes and immobile superoxide anions.[47] Interestingly, an experimental correlation between photocurrent and the concentration of charge carriers in blended P3HT:PCBM was noted by Guerrero *et al.*, who found $J_{sc} \propto n^{-0.14}$.[69] Clearly, the oxygen generation or enhancement of bandgap residing states has a significant effect on the long term stability of these devices. Please note, the topic of degradation is vast and, though heavily related, beyond of the scope of this review. Many excellent reports can be found in the literature, we have chosen only to comment on a select few which indicate some effects of degradation on the trap states. A full review on OPV degradation can be found elsewhere.[87]

Turning to the yet deeper (*ca.* 380 meV) band discussed above, details as to its formation have been provided by Nalwa *et al.*, who applied the CF method to ITO/PEDOT:PSS/P3HT:PCBM/Al cells with active layers spun at different rates.[22] Each spin rate produces a different film thickness, which greatly alters the drying time, and thereby, morphological ordering.[61] Many prior reports had shown the promotion of self-assembly improves OPV performance through enhanced morphology, carrier mobility, *etc.*[61] Thus, the authors set out to study the dependence of the deep-trap energetic profile on the film growth-rate.[22] The group found that films spun at lower speeds (thicker and slower drying) are more ordered and contained nearly a magnitude less deep traps than those spun at higher speeds (thinner and faster drying). Defect densities of 3.3×10^{15} and 2.1×10^{16} cm^{-3} and mean energies of 360 and 380 eV ($\nu_0 = 1 \times 10^{12}$ s^{-1}) were found for devices with active layers spun at 400 and 1000 rpm respectively.[22] If the assumed attempt-to-escape frequency is accepted, this band closely matches the above reports and the data indicates the defect has origins in intrinsic structural impurities. A similar case was also shown by Sharma *et al.* for CuPc based devices.[88]

Seemann *et al.*'s impedance measurements also gives interesting insights into this deep band.[47] As seen in Fig. 14, an increase in the capacitance and a corresponding decrease in the parallel resistance with exposure to synthetic air (20% O_2, 80% N_2) was found – especially in presence of light.[47] They attributed this observation to an increase in extrinsic charges induced by oxygen doping. Pushing the analysis further, we note the response of this increase is frequency dependent. In accordance

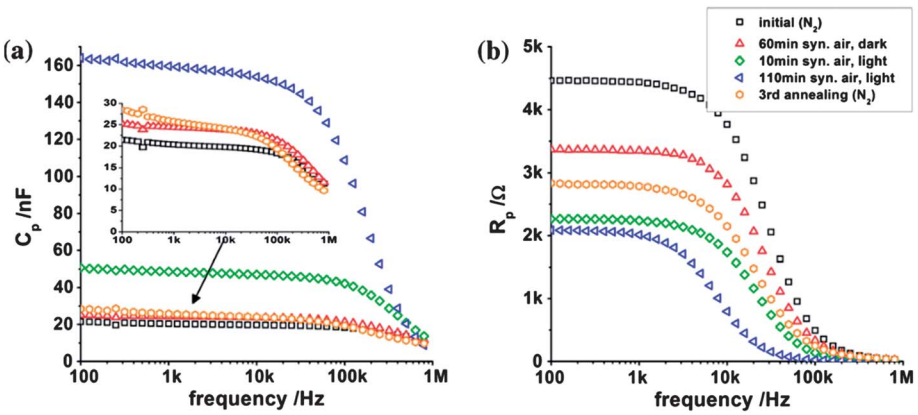

Fig. 14 Spectrally resolved device capacitance (left) and device resistance (right) extracted from the admittance of a typical solar cell measured under nitrogen in the dark after exposure of the cell to different degradation conditions. The data are normalized to the respective values at 100 Hz before the first exposure of the device to synthetic air. Reprinted from publication ref. 47, Copyright [2011], with permission from Elsevier.

with the CF interpretation summarized in Appendix section 8.5, this may indicate oxygen induced changes in the *ca.* 300–500 meV deep-defect distribution.

To test this hypothesis, we have fabricated standard cells from a P3HT:PCBM blend (ITO/PEDOT:PSS/P3HT:$PC_{60}BM$/Al) and monitored the frequency dependent capacitance as a function of air exposure (Fig. 15a). The values are normalized to the geometric capacitance and a combination of parallel (C_P) and series (C_S) parameters were used.[89] The data qualitatively matches Fig. 14, with a near plateau at lower frequencies (traps responding) and a decrease towards the geometric capacitance at high frequencies (no traps responding). The data was analyzed according to eqn (20) and fit with a Gaussian distribution (Fig. 15b). For reference, an attempt-to-escape frequency of 5×10^{10} s^{-1} was used. The resulting distribution was centered at 320 meV above the HOMO with a standard deviation around 45 meV. Indeed this band is the same as that of Boix, Nalwa and the like; the noted shift stems only from the chosen characteristic frequency. As predicted, the deep trap concentration was strongly influenced by air exposure, indicating this band has origins in both intrinsic and extrinsic sources. This dependence on air exposure is not so surprising considering the earlier sub-gap optical absorption experiments, which showed oxygen induces, or at the least augments, a large distribution of states throughout the mid-gap.

Of course, impurities from synthesis residuals cannot be forgotten. As discussed in Section 3.4, contamination during material synthesis can have detrimental effects on device parameters. In the case of a palladium catalyst, this has been evidently highlighted for P3HT:PCBM based BHJ devices.[72,73] In their work on the development of a quality control measurement tool, Troshin *et al.* investigated the effects of an intentional addition of tetrakis(triphenylphosphine)palladium(0) ($Pd(PPh_3)_4$) to P3HT:PCBM cells.[72] 0% to 10.5% by weight addition of palladium was investigated. As can be seen in Fig. 16, the transition metal has a dramatic effect on the solar performance parameters. With an increasing impurity concentration open circuit voltage, short circuit current and fill factor were rapidly degraded. Even at palladium concentrations as low as 0.07% a reduction in performance was noted.[72] A similar case has also been found for palladium additions in higher efficiency organic solar cells (based on PTB7 (poly[[4,8-bis[(2-ethylhexyl)-oxy]benzo[1,2-*b*:4,5-*b*′]dithiophene-2,6-diyl][3-fluoro-2-[(2-ethylhexyl)carbonyl]thieno[3,4-*b*]thiophenediyl]])), where the degradation in performance parameters in devices containing 5% ($Pd(PPh_3)_4$) was directly linked to greater trap-assisted recombination.[18] This, of course, is in nice agreement with the works discussed in Section 4.3 – that is, higher trap densities leads to a dominance of trap-assisted recombination losses. Extending to contaminants other than palladium, such a thought is further supported. In a work by Leong *et al.*, trace concentrations of (MePT)DTS($PTTh_2$) in the molecular material *p*-DTS($PTTh_2$)$_2$ were found to originate from the synthesis process.[16] Through generation and recombination studies, the authors found evidence of more energetic trap states in the impure films, even at very low contamination levels. As a result, this extrinsic impurity limited the PCE of BHJ structured cells (ITO/molybdenum oxide/*p*-DTS($PTTh_2$)$_2$:$PC_{70}BM$.Al) to *ca.* 3.0%.[16] Indeed, OPV devices based on more purified *p*-DTS($PTTh_2$)$_2$ material exhibited a substantially higher PCE at *ca.* 6.5%, again highlighting the importance of purifying these types of extrinsic impurities.

Evidently, the same primary sources inducing defects in neat films have similar effects on blended systems. Defect bands have been shown to be heavily influenced by the degree structural ordering as well as by exposure to oxygen/moisture. Impurities introduced during material synthesis also clearly

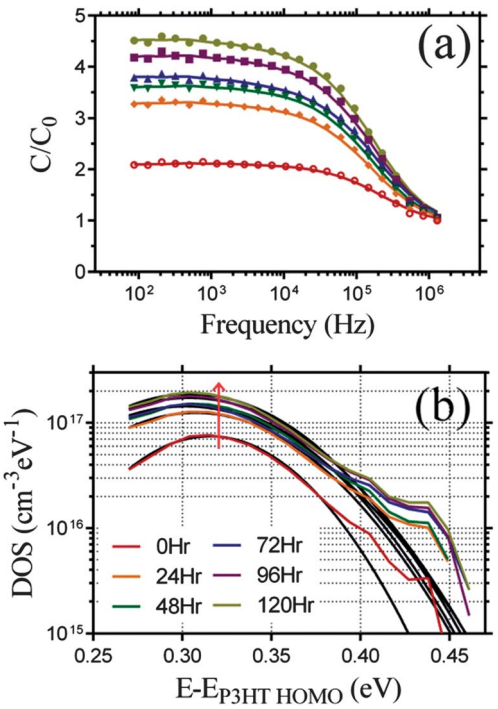

Fig. 15 (a) CF normalized to geometric capacitance (*ca.* 2.4 nF) in dark at 300 K, 0V_{DC} and 25 mV rms AC as a function of air exposure and (b) calculated tDOS fit by a Gaussian distribution. Arrow shows trend for increasing air exposure time.

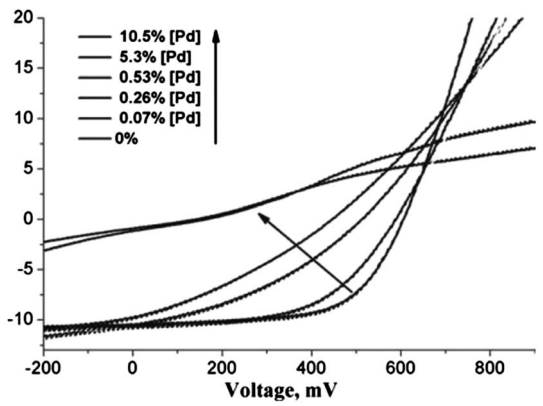

Fig. 16 Effect of [palladium] impurities on the *I*–*V* characteristics of P3HT/PCBM organic solar cells. Reprinted with full permission from ref. 72. Copyright [2010], John Wiley and Sons.

play a role; though it is unclear at this point which of the above-discussed mid-gap levels can be attributed to residuals such as palladium. Nonetheless, this highlights the path towards lowering electronic defects in OPV devices likely includes structural ordering, the removal and minimization of oxygen exposure and the purification of raw materials. These will be further expanded in Section 6, but first, we tie up some loose ends.

5. Identification and characterization: miscellaneous loose ends

Before moving on to a discussion on trap mitigation, this section is used to tie up loose ends pertaining to the important and ubiquitous capacitance measurements. Much work has gone into interpreting the capacitive response of inorganic cells and we suspect the same will prove true for organics. The goal of this section is to provide some contrast to the works above and direct the reader toward alternate interpretations as well as known issues.

First, the dual MS slope commonly seen in CV measurements must be revisited. The works above interpreted this change in slope as either spatial contributions from an inhomogeneous doping profile or energetic contributions from a deep defect band. However, other interpretations have been applied to organic CV profiles and should be considered. One such explanation was provided by Nolasco *et al.* in 2010 as well as Ecker *et al.* in 2011.[85,90] In the latter, the BHJ CV data clearly contains two regimes with differing slopes. The first, at low forward/reverse bias, was attributed to the 'donor phase', while the second, at moderate reverse bias, was attributed to the 'acceptor phase'. Meaning, in region (i), the authors assume $N_{D\ PCBM} \gg N_{A\ P3HT}$ – creating a one-sided junction where the MS slope is governed by $N_{A\ P3HT}$. In region (ii), as the P3HT depletes, $N_{D\ PCBM}$ begins to dominate and a new slope emerges. The authors find $N_A^-{}_{P3HT} = 1.0$ to 3.0×10^{16} cm^{-3} and $N_D^+{}_{PCBM} = 0.5$ to 2.5×10^{18} cm^{-3}, both in line with the expected values. Aside from highlighting an alternative interpretation of the dual slope, this also brings about an interesting discussion on which junction in the BHJ structure is being probed by the capacitance experiments. It is clear that Ecker *et al.* have assumed the donor–acceptor junction, much like a classical p–n treatment. However, others have indicated that the Schottky junction between the polymer and cathode is being measured.[39,77] Of course one might also consider contributions from a Schottky junction between the fullerene and anode, which is expected to form with proper energy alignment and moderate doping.[59,91] Though, more heavily doped fullerenes may show essentially ohmic behavior.[59] Some combination thereof might also be considered. More work is required to pinpoint the exact nature.

Similarly, alternative interpretations of CF have surfaced. The formalism used in the above reports was presented by Walter *et al.* in 1996.[92] However, Cohen and Lang have also discussed the dynamic response of Schottky barriers and interpretations of their model have been applied in organic works.[93–95] Most interesting is that by Reis *et al.* in which capacitance measurements as a function of both frequency and temperature were analyzed using a derivation[96] of the model described by Cohen and Lang as well as that described by Walter *et al.* (Au/doped-polyaniline/Al structure).[94] Interestingly, a comparison of the density of defects derived from each model showed they were in good agreement.[94] Being that both yield a similar concentration, it is our interpretation that the Mencaraglia *et al.* application of the Cohen formalism is advantageous as the Fermi-level and Debye length [among other parameters] are easily found; while the Walter formalism is advantageous as an energetic profile of the tDOS is obtained. The latter is typically preferred, though a best case scenario may be represented by an analysis and comparison of both models. Of course, one must also ensure the assumptions of each model are suitable for the material system at hand.

Lastly, potential issues in the MS CV analysis must be mentioned. In 2011, Mingebach *et al.* reviewed the validity of determining the built in voltage of OPV devices *via* the MS method.[97] Though this paper itself does not directly discuss defects, its conclusions are important to examine as the Walter *et al.* CF method relies on an accurate value of V_{bi}, which is typically determined by MS analysis. Citing differences in the MS measured and theoretically expected V_{bi}, the interpretation of the MS intercept as the built in voltage was questioned. Further, a thickness dependence in the MS measured V_{bi} was found (Fig. 17); another indication the measurement may not be accurate.[97] These points, coupled with temperature-dependent measurements, caused Mingebach *et al.* to conclude that the classical idea of the MS intercept may not be applicable to BHJ based OPVs. Kirchartz *et al.* further studied this concept in 2012.[98] The group started with the question of how OPV devices can have a V_{bi} significantly lower than V_{oc} (as measured from CV MS), but still produce efficient cells with practical FFs.[98] Through simulations and experimental work, the authors

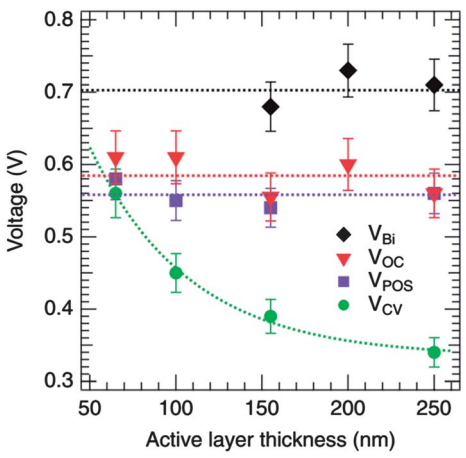

Fig. 17 V_{bi} (black diamonds, determined as shown in Fig. 5 [of the original article]), V_{oc} (red triangles), V_{pos} (purple squares), and V_{cv} (green circles) for P3HT:$PC_{61}BM$ bulk heterojunction solar cells with varying active layer thickness. In contrast to V_{oc}, V_{pos}, and V_{bi}, V_{cv} shows a clear dependency on the active layer thickness (increases with decreasing thickness) and approaches V_{pos}. The dotted lines are guides to the eyes and mark the mean values of the corresponding potentials resp. an exponential fit to V_{cv}. Reprinted with permission from ref. 97. Copyright [2011] by the American Physical Society.

showed that MS analysis on OPV devices is highly sensitive to both film thickness and the inherent doping level.[98] In too thin or lowly doped films, charge carriers injected near the electrodes cannot be neglected. This breakdown in the depletion approximation greatly affects the accuracy of the capacitance data, and thereby, may cause errors in the analysis. Most notable is an apparent decrease in N_A^- with increasing film thickness. In the case of a film doped to 5×10^{15} cm^{-3}, it is only at thicknesses greater than *ca.* 150 nm that the measured density of acceptor states saturates to the appropriate level and the method is considered generally applicable. Similar to Mingebach *et al.*,[97] this thickness dependence was also seen in V_{bi} – a result directly connected to the apparent decrease in doping. As a result of the work, the authors assert that CV analysis for the accurate determination of N_A^- may only be appropriate when films are thick and/or more heavily doped, while the accurate determination of V_{bi} may be difficult, no matter the material parameters.[98] Of course, with the assumption that these capacitance measurements target only the polymer–cathode Schottky interface, one might consider that the obtained V_{bi} relates only to that particular junction and does not set an upper limit on the photovoltaic voltage.[99]

6. Defect mitigation

With some understanding as to the presence and characteristics of trap sites in OPV devices, we now look at some recent efforts to mitigate. We begin with a discussion on structural ordering. Much work has gone into studying the crystallization kinetics of organic materials and blends thereof. Several techniques, including thermal annealing, solvent annealing and solvent additives, have been adopted or developed to promote self-organization in OPV devices.[61] When employing these techniques, most groups cite a higher degree of crystallinity coupled with enhancements in physical parameters (*e.g.* mobility) as well as photovoltaic performance. Though most of these reports do not show any direct measurements of trap states, this strongly indicates that structural defects are being reduced. In the case of deeper levels, this idea is fully supported by Nalwa *et al.*'s and Sharma *et al.*'s growth rate works, as discussed above.[22,88] Further, when comparing the apparent hole concentrations and processing conditions of Dennler *et al.*'s and Li *et al.*'s works, some evidence was presented that the case is similar for shallower levels and doping.[13,60] This readily points out the obvious – one avenue towards trap reduction in OPV devices is promoting more order in the film structure. Though this assertion is seemingly unexciting, it represents a vast and important area of research. Numerous reports on the self-assembly topic can be found in the literature,[100] and their continued application and development will be important to trap mitigation in both current and future OPV materials.

In addition to crystallinity affects, thermal treatments have also been shown to promote the desorption of oxygen, reversing its effects on the ionized acceptor impurity concentrations.[15,42,44,46,47,76,101] One such example is shown by Seemann *et al.* in Fig. 18.[47] Clearly, the extrinsic impurities induced by synthetic air are readily reduced through thermal treatment.

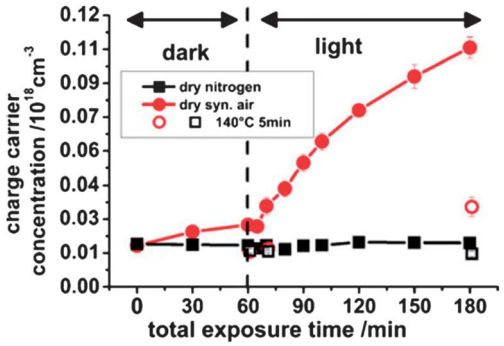

Fig. 18 Charge carrier concentrations calculated from the data of Fig. 5 [of original article] by using eqn (2) [of original article]. Reprinted from publication ref. 47, Copyright [2011], with permission from Elsevier.

Glatthaar *et al.* found a similar reduction in doping and noted an improved rectification for P3HT:PCBM BHJ cells after post-production thermal annealing under forward biasing.[76] This is further supported by Nam *et al.*'s aforementioned modeling work.[75] The authors found that a post-production treatment of their air-processed devices significantly reduced oxygen content in the active layer blend. The group proposed this lead to a reduction in the oxygen-related impurities, and thereby, an enhancement to the short circuit current.[75] Hintz *et al.* offer further details as to this desorption through photoelectron experiments.[42] After monitoring binding energies and oxygen content through a series of exposure/annealing cycles, the group identified two oxygen species: one reversible and one irreversible. The former correlates to noted changes in the material doping and was found to be only a small fraction of the total oxygen content.[42] This is attributed to physisorbed oxygen which forms a CTC as previously discussed. The latter existed in higher numbers and was attributed to oxygen contained within photooxidation products.[42] They believe this bound species is contained to electrically isolated molecular sites, and thereby, the electronic structure of the π-system is not largely altered.[42] Seemann *et al.* noted a similar irreversible aspect in their oxygen degradation studies, attributed to photochemical oxidation.[47] They believe this irreversible portion may induce a slight increase in the mobile hole concentration (Fig. 18), and thereby, decrease carrier mobility.[47] It is worth noting that although moderate temperatures (>100 °C) may be needed for the rapid removal of oxygen,[101] desorption is still expected to occur even at room temperature, albeit on a much longer timeframe.[44]

Along with structural and oxygen induced defects, impurities from material synthesis must also be carefully mitigated. Not only would this relieve the performance degradations discussed in Sections 3.3 and 4.5, but also may be advantageous for better device reproducibility. It is thought that batch-to-batch variations in the residual synthesis impurities are a significant factor affecting the poor batch-to-batch reproducibility of OPV opto-electronic properties,[18,72] making the mitigation of such impurities a promising avenue towards more consistent processing. Unfortunately, the detection of trace (*e.g.* <1% by weight) synthesis impurities, and thereby the estimation of material

purity, has proven challenging with traditional methods.[16,18,72,102] Though, Nikiforov *et al.*'s recent work shows synchrotron X-ray fluorescence as a promising measurement for identifying trace residuals and quantifying their concentrations.[18] Making matters worse, purification – especially noted for the case of palladium – is notoriously difficult as decomposition of this transition metal catalyst forms nanoparticles which can tightly bind to the backbone of conjugated polymers.[18,72,102] Fortunately, the works of Krebs *et al.* have begun to tackle this issue.[17,102,103] In the initial PPV based work discussed in Section 3.4, the authors undertook multiple micro-filtrations in order to remove the palladium contaminant.[17] A two fold increase in film resistance (30 to 60 Ω) was achieved as the shunt paths induced by the palladium nanoparticles were removed. With a subsequent boiling of the polymer in a ODCB : triphenylphosphine mixture and a precipitation with methanol, the resistance was further increased to 100 Ω – though, still short of the 150 Ω found for the more palladium free case.[17] This work was then built upon by treating palladium contaminated PPV (as well as two other polymers) with a azothioformamide derivative to dissolve the residual.[102] The authors found an impressive drop in palladium content (17 860 to <0.10 ppm) coupled with a 300× improvement of film resistance.[102] A year later, the group then pushed this idea further to demonstrate the ability of azothioformamide derivatives to remove other transition metals (*i.e.* palladium, platinum, copper and nickel) from contaminated organic products.[103] More information on synthesis, purification and the associated challenges can be found throughout the literature.[104,105]

Wang *et al.* have tackled defect mitigation from a different point of view.[23] Taking cues from trap-rich amorphous silicon, which is typically hydrogenated to reduce the concentration of defects, Wang treats P3HT with a cation donor, dimethyl sulfate.[23] The polymer solution was reacted with the donor in the hope that cations would be donated to the polymer backbone and annihilate negatively charged defects. As a byproduct, the authors asserted an unbound sulfate counterion would be formed, though, it is expected that this 'defect' would have less influence on electrical properties.[23] As such, one would expect improvements in the abovementioned deficiencies created by charged defects (charge mobility, exciton diffusion length, *etc.*). The authors showed just that through time-of-flight (mobility) and fluorescence (exciton diffusion length) measurements.[23] One might be inclined to argue that the chemical treatment could act much the same as a solvent additive – affecting crystallization kinetics and film morphology, which could bring about the same type of improvements.[61] However, optical absorption and X-ray diffraction measurements revealed no substantial changes to structure and morphology.[23] Though photovoltaic improvement was meager, photostability was dramatically improved with this treatment.

This work was extended by Liang *et al.* in 2009.[24] Here, the authors furthered the study on dimethyl sulfate and expanded to include a second regent, lithium aluminum hydride (LAH). To be thorough, the study also mentioned treatments with sodium borohydride, sodium methoxide and methyl iodide, as well as treatments on PPV, which all gave consistent results.[24] Similar to the previous work, mobility and exciton diffusion length enhancements were noted, with LAH producing the largest increases – 17 fold for mobility and two fold for exciton diffusion.[24] Photostability was also again improved. Interestingly, the zero-field dark conductivity increased by a factor of five for dimethyl sulfate, but increased only slightly in the case of LAH treatment. Thereby, the mobile hole density doubled for dimethyl sulfate treatments, but decreased by a factor of 13 for LAH. The estimated total defect density dropped by an order of magnitude in the case of dimethyl sulfate (1×10^{19} cm^{-3} to 1×10^{18} cm^{-3}) and by nearly three orders of magnitude for LAH (to 3×10^{16} cm^{-3}),[24] directly highlighting the effectiveness of the mitigation technique.

A similar concept has also been applied to mitigate electron traps in PPV and, more recently, C_{60}.[106,107] In the latter, the ruthenium(pentamethylcyclopentadienyl)(1,3,5-trimethylbenze) dimer $[RuCp^*(mes)]_2$ was added to the trap-rich fullerene *via* co-evaporation.[106] Thereby, an extra, molecular n-type doping was introduced into the system, traps were filled and passivation was achieved. Direct evidence of this is presented in Fig. 19, where the peak HOMO position and work function are plotted *versus* the doping molar ratio (MR).[106] Clearly, a trend in the energetic positions is seen with increasing dimer doping. The authors assert such a trend is consistent with the Fermi-level moving through a distribution of trap states towards the LUMO manifold.[106] Around a MR of *ca.* 6.0×10^{-3}, the trend merges with the expected trap-free slope, giving some quantification as to the minimum doping density needed for controlled passivation. Through this process, both conductivity and mobility were vastly improved – indicating potential improvements for OPV performance. Similar data has been shown for other dopant materials in C_{60} systems.[108,109] Further, when recalling the work of Garcia-Belmonte *et al.* (Fig. 13) it is remembered that a decrease of electronic states in the acceptor material alleviates Fermi-level pinning and enhances the achievable

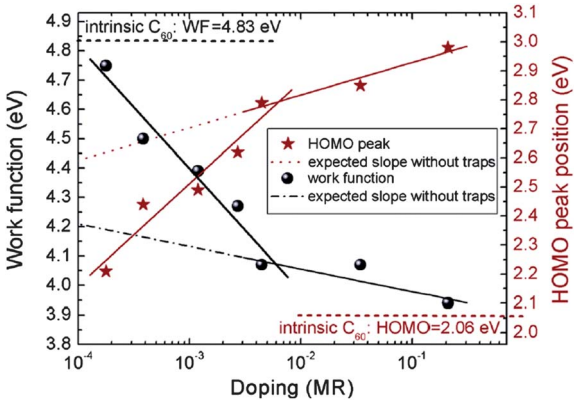

Fig. 19 Change in work function and HOMO peak position with respect to the Fermi level upon doping. Deduced from the UPS spectra given in Fig. S2 [of the original article] in the SM [31; of the original article]. Because of the broadening of the HOMO feature at high doping, the HOMO position is given by the peak value. The corresponding values for the intrinsic C_{60} film are given by the top and bottom dashed horizontal line, respectively. Reprinted with permission from ref. 106. Copyright [2012] by the American Physical Society.

V_{oc}.[35] This enhancement should also remain true for trap passivation as detailed here. In fact, such a case with donor materials was hinted at by Boix *et al.*, who incidentally found that inverted cells had four times the p-type doping and an increased V_{oc} when compared to a regular structure.[110] As a result of the excess holes, E_{Fp} was expected to shift towards the HOMO, thereby increasing the achievable open-circuit voltage.

7. Conclusions

7.1. Synopsis

In summary, the current state of the identification, characterization and mitigation of bandgap residing trap levels in organic photovoltaic devices has been reviewed. To date, several techniques have been leveraged to study these mid-gap states. Atop this list are optical (PSD, UV-vis), capacitance (CV, CF, DLTS) and current (TSC, SCL modeling, Poole–Frenkel modeling) measurements and each has provided important pieces to the overall picture. A compilation of the defect literature to date depicts pure OPV materials as disordered semiconductors with a seemingly continuous distribution of both energetically shallow and deep trap bands. Upon blending these pure materials to create the modern day bulk heterojunction, energetic disorder increases and new trap bands appear. These states have been shown to stem from both intrinsic (*e.g.* structural disorder) and extrinsic (*e.g.* oxygen, synthesis contaminates) sources and it is quite clear that such states can have profound effects on, if not completely control, the electronic properties and long term stability of OPV devices. Several works highlighting the drastic effects trap states can have on OPV performance have evidently shown this – citing enhanced trap-assisted recombination, Fermi-level pinning, space-charge effects and the like. Though these mid-gap traps have a large negative impact, it should also be remembered that they can give an advantageous inherent doping, improving conductivity and interfacial electric fields. Lastly, initial works centered on defect removal were presented. Structural ordering, the control of oxygen absorption, material purification and passivation have been shown to be promising mitigation techniques. Evidently, continued progress in understanding the nature, sources, affects and mitigation of the defects in both current and future materials will be crucial to the optimization of this promising technology.

7.2. Outlook

Looking forward, several avenues of future work can be identified. Of course, it will be of upmost importance to extend the methods and works discussed above to probe and better understand the complete trap profiles of the new, promising OPV systems. Trap-related conclusions made for one organic material set may not be directly applicable to the next – especially considering the potential for vast differences in the synthesis impurity concentration, inherent structural disorder, sensitivity to oxygen/moisture, *etc.* – truly highlighting that trap effects cannot be overlooked. It is plain to see that the characteristic parameters of the defect distribution(s) as well as their origin(s) must be understood such that these future, high efficiency materials can be further optimized through a reduction of these electronic states. As a general approach, we align with and build upon the idea of Gregg.[27] OPV materials should first be pushed towards a more ideal, intrinsic state through structural ordering, the removal of oxygen states, material purification, *etc.* Subsequently, remaining traps might then be further reduced through chemical passivation and the electronic properties rebuilt through a controlled, extrinsic doping. Though it may be impossible to completely rid these systems of electronic traps, their reduction by even an order of magnitude (or more) will likely prove fruitful.

To accomplish this goal, measurement as well as mitigation techniques must be continually developed. Defect measurements and their interpretations should be refined to ensure validity and accuracy of the identified bands. For example, consider the ubiquitous capacitance measurement – specifically CV and CF. When the deep-level states outnumber that of the shallow, deep-trap occupancy must be considered and the concept of a well-defined, fully depleted space charge region does not exist. In turn, the depletion capacitance is defined by $C_d = \varepsilon_s A/\langle x \rangle$, where $\langle x \rangle$ is the first moment of charge response.[63] Allusions to this concept have already been made in the above discussion and the Appendix. Walter *et al.*, Kimerling, Cohen and Lang and several others have contributed important works towards the effort of interpreting capacitance measurements in such cases – many of which have already been applied to OPVs. To push the OPV analysis further, drive level capacitance profiling (DLCP) might be considered to help further sort things out.[63] This capacitance based technique was pioneered by Michelson and Cohen and is somewhat analogous to CV and CF in that it assesses both carrier density and energetic trap states.[63,111,112] However, it does so with higher accuracy, insensitivity to contact interfacial states and without the knowledge of V_{bi} and W.[112] Thus far, no reports applying this technique to OPV devices have surfaced. In light of the issues with interpreting CV data, coupled with the possible issues in accurately determining V_{bi} and N_A^- from MS analysis, DLCP represents a promising avenue for future, accurate capacitance measurements and the characterization of trap bands in OPV materials.

Careful characterization deeper, towards the midgap of the material bandgaps – a region which likely holds performance altering states – should also be considered. In the donor portion, for example, the above discussion shows reports identifying and characterizing bandgap residing trap states only to *ca.* 0.50 eV above the polymer HOMO. In a typical polymer bandgap (*e.g.* 2.0 eV) this represents only the quarter-gap. Owing to the large amount of energetic disorder present in these systems, deeper states are likely present and may contribute to a trap-assisted recombination mechanism or facilitate space charge effects. Limitations in the practical applications of the measurement techniques discussed in the Appendix, however, make the accurate characterization of this energy regime somewhat challenging (*e.g.* high temperature limitations for thermal based techniques or low frequency limitations in capacitance based techniques). Nonetheless, overcoming such challenges and accurately identifying and

characterizing defects in this energy will be important. Initial reports on this topic are beginning to surface.[113]

Lastly, mitigation techniques must be furthered. Though several works have already noted some trap reduction and a corresponding improvement in electronic properties, much scope in this area left to explore. Comprehensive reports systematically highlighting a decrease in trap concentrations at specific energies coupled with an increase in photovoltaic performance would greatly contribute to the science of OPVs. Further, combining mitigation techniques (*e.g.* thermal treatments with chemical passivation) is an interesting avenue to consider. And, of course, enhancing useful levels with a controlled addition of dopants also seems promising.

8. Appendix: measurement techniques

8.1. Thermally stimulated current (TSC)

In a basic sense, the conventional TSC method can be understood as follows. The sample is first cooled to cryogenic temperatures and excess charge carriers are generated (*e.g.* optically or through a voltage bias) to induce a long-lived filling of the trap states. Subsequently, the sample is slowly heated at a linear rate, stored charges are thermally emitted and the stimulated current is monitored. Thereby, a current *versus* temperature (*e.g.* Fig. 3) spectrum is generated. Both the concentration and mean energy of the dominate trap can then be calculated. The former is quantified by,

$$\int_{\text{total}} I_{\text{TSC}}\mathrm{d}t \leq qN_{\text{T}} \tag{3}$$

where q is the elementary charge.[114,115] As can be seen, this technique only gives a lower limit of the total trap density. Recombination between thermally released electrons and holes can cause some stimulated current to be 'lost', lowering the measured trap states. Further, incomplete trap filling and/or limited detrapping can also lower the measured results. The mean trap energy is quantified by,

$$E_{\text{T}} = k_{\text{B}}T_{\max}\ln\left(\frac{{T_{\max}}^4}{\beta}\right) \tag{4}$$

where k_{B} is the Boltzmann constant, $T_{\max}$ the temperature at the current peak and β the heating rate.[116]

8.2. Fractional thermally stimulated current (FTSC)

An extension of the conventional method in which fractional heating cycles are used to further resolve the temperature/energy spectrum is known as T_{start}–T_{stop} or fractional TSC (Fig. 20).[117] As usual, the sample is first cooled to a minimum temperature (T_{start}) and then trap filled. However, the sample is next scanned (heated) to an intermediate end temperature (T_{stop}), which is less than the final temperature of interest – 'prerelease'. Subsequently, the sample is again cooled to T_{start} and then, without a second trap filling, scanned to said final temperature – 'main run'. This fractional cycle is then repeated for increasing T_{stop} temperatures. Assuming the initial rise of the fractional TSC interval (Fig. 20) is described by a Boltzmann

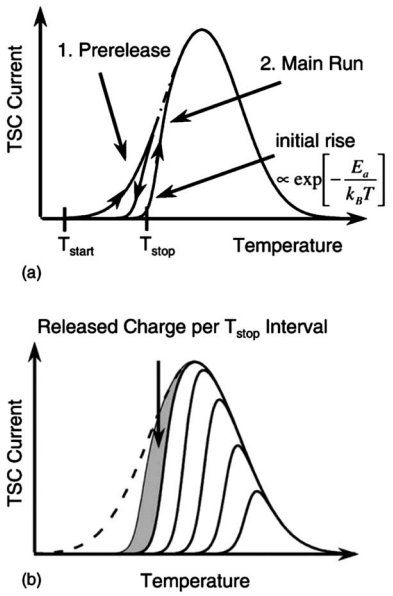

Fig. 20 Schematics of the T_{start}–T_{stop} method: (a) the basic cycle consists of two individual TSC scans and (b) the whole measurement is a replication of basic cycles with different T_{stop} temperatures. The activation energy of the initial rise describes the energetic trap depth, while the shaded area resembles the released charge.

activated process, the activation energy for each T_{stop} can be found *via* the 'initial rise method', which is quantified by,

$$I_{\text{iTSC}} \propto \exp\left(\frac{-E_{\text{T}}}{k_{\text{B}}T}\right) \tag{5}$$

where I_{iTSC} is the current of the initial rise and T the temperature.[117,118] The activation energy can then be coupled with a concentration, calculated from eqn (3), to build an energetic tDOS.

8.3. Space charge limited (SCL) current modeling

Dark current–voltage characteristics can also be examined to determine trapping parameters. Neglecting diffusion and assuming a constant mobility, the current density in a single carrier, p-type material is described by,

$$J = q\mu_{\text{p}}F(x)p_{\text{f}}(x) \tag{6}$$

where μ_{p} is the hole mobility, $F(x)$ the spatial distribution of the electric field and $p_{\text{f}}(x)$ the spatial density of free holes.[56,119,120] The spatial distribution of the electric field is given by the Poisson equation,

$$\frac{\mathrm{d}F(x)}{\mathrm{d}x} = \frac{q}{\varepsilon_{\text{s}}}\left[p_{\text{f}}(x) + p_{\text{T}}(x)\right] \tag{7}$$

where ε_{s} is the semiconductor permittivity and $p_{\text{T}}(x)$ the spatial density of trapped holes, which is defined by,

$$p_{\text{T}}(x) = \int_0^\infty g(E)f(E, E_{\text{F}}, T)\mathrm{d}E \tag{8}$$

where $g(E)$ is the DOS and $f(E,E_{\text{F}},T)$ the Fermi function for occupation.[56,119,120] Thus, with the definition of $E_{\text{F}}(x)$,[119]

numerical integration yields a current density, which can be coupled to a voltage *via*,

$$V = \int_0^d F(x)\mathrm{d}x \tag{9}$$

where d is the sample thickness.[56] Extensive modeling as such yields information on the energetic distribution. If an exponential or Gaussian distribution of traps is assumed such that $p_f < p_T$, some further simplifications can be made. In the case of an exponential distribution,

$$g(E) = \frac{N_T}{k_B T_T}\exp\left(\frac{-E}{k_B T_T}\right) \tag{10}$$

where T_T is the characteristic temperature, the drift-only current density is readily approximated by,

$$J = q^{1-l}\mu_p N_V \left(\frac{2l+1}{l+1}\right)^{l+1}\left(\frac{l}{l+1}\frac{\varepsilon_s}{N_T}\right)^{l}\frac{V^{l+1}}{d^{2l+1}} \tag{11}$$

where V is the voltage and $l = T_T/T$.[121] When a Gaussian distribution is assumed,

$$g(E) = \frac{N_T}{\sqrt{2\pi}\sigma_T}\exp\left(-\frac{(E-E_T)^2}{2{\sigma_T}^2}\right) \tag{12}$$

two considerations must be made. For shallow trap centers, the current density is approximated by a modified Mott–Gurney law,

$$J = \frac{9}{8}\varepsilon_s\mu_p\theta\,\frac{V^2}{d^3} \tag{13}$$

where θ is a scaling factor[122] and $\mu_p\theta$ represents the effective mobility dependent on the ratio of free to trapped charges. For deep trap centers, the current density is again approximated by eqn (11), but with a modified exponent (l') and concentration of trap states (N_T').[122] In contrast to these simplifications, others have gone the opposite direction to employ more complex modeling which accounts for diffusion current as well as electric-field and carrier concentration dependencies of the mobility.[123] It should also be pointed out that the use of SCL and modified SCL models is seemingly ubiquitous in the device literature, however, its application to π-conjugated polymers has been called into question.[40]

8.4. Capacitance *versus* voltage (CV)

Capacitance measurements have long been employed to study mid-gap states in semiconductor devices. CV measurements exploit the existence of a depletion region, formed at a semiconductor junction. Consider, for example, an ideal p-semiconductor/metal Schottky junction. In such a case the depletion capacitance is defined by,

$$C_d = \varepsilon_s A/W, \tag{14}$$

which can be linearized to reveal the well-known Mott–Schottky (MS) relation,

$$\frac{1}{C^2} = \frac{2}{A^2 q\varepsilon_s N_A}(V_{bi} - V_{app}) \tag{15}$$

where W is the depletion width, N_A is the acceptor impurity density, V_{bi} the built in voltage and V_{app} the applied bias.[63] Strictly speaking, a better approximation replaces V_{bi} with V_D, where V_D is the diffusion potential and related to V_{bi} by $qV_{bi} = E_F + qV_D$.[124] Nonetheless, a plot of $1/C^2$ *versus* the applied DC voltage produces a straight line with the slope related to N_A and the intercept to V_{bi}. In an inhomogeneously doped material, the spatial distribution of acceptor states can be determined through the related profiler equation,

$$N_A(x) = \frac{C^3}{q\varepsilon_s A^2}\frac{\mathrm{d}V}{\mathrm{d}C} \tag{16}$$

where x is the spatial distance from the junction. These equations, however, represent an idealization of a *perfect*, pure material. When deep defects are present, especially if they are in large numbers, several considerations must be made to properly interpret capacitance data. Most notably, defect contributions to the capacitance as a function of DC bias as well as AC frequency must be accounted for. The former is briefly summarized here and the latter is addressed in Appendix section 8.5.

The influence of deep traps on CV measurements was discussed by Kimerling in 1973.[64] Though many considerations must be made to accurately employ the interpretation, the formalism can be summarized as follows. In the popular case when trap emission ($e_{n,p}$) is slower than the AC measurement frequency (ν_{AC}) the trap is considered frozen and does not contribute to the capacitance as a function of the small-signal oscillation. However, if trap emission is faster than the change in DC voltage (ΔV_{DC}), the trap can alter its occupancy over the course of the voltage sweep, and thereby, contribute to the capacitance as function of DC bias.[64] In such a case, $\nu_{AC} > e_{p,n} > \Delta V_{DC}$ and the 'N_A' measured by eqn (15) or (16) actually represents,

$$N(x) = N_T(x_T)\left[1 - \frac{W - x_T}{W}\right] + N_A(W) \tag{17}$$

where x_T is the spatial demarcation where E_T is within $k_B T$ of E_F and $W - x_T$ is assumed constant.[63,64] Thus, when x_T is small, $N_A(x)$ indeed represents N_A. However, for larger values of x_T (note, x_T is always less than W), $N_A(x)$ more closely represents $N_A + N_T$.

8.5. Capacitance *versus* frequency (CF)

Deep defects states can also contribute to the capacitance measurement through a dynamic response to the AC small-signal. This forms the basis for capacitance *versus* frequency (CF) measurements, which were discussed by Walter *et al.* in 1996.[92] CF, also termed admittance spectroscopy, is a frequency differential in which the junction is maintained at a steady state DC voltage and the modulation speed of the small-signal AC measurement is swept to include (or exclude) trap states. The thermal emission rate of a trap state in a p-type semiconductor is quantified by,

$$\frac{1}{\tau_p} = e_p = N_V v_{th}\sigma_p \exp\left(\frac{-E_A}{k_B T}\right) \tag{18}$$

where N_V is the valence band density of states, ν_{th} the thermal velocity, σ_p the capture cross-section, E_a the trap activation energy.[63,80] In inorganic device physics, with an assumption that $\nu_{th} \propto T^{1/2}$, $N_V \propto T^{3/2}$ and σ_p independent of T, the prefactor in eqn (18) is commonly written in terms of T^2 – *e.g.* 'ζT^2' or '$\Upsilon \sigma_p T^2$', where $\zeta = N_V \nu_{th} T^{-2} \sigma_p$ and $\Upsilon = N_V \nu_{th} T^{-2}$ respectively.[63,80] Alternatively, the prefactor is often written as a single, temperature independent parameter, ω_0, termed the attempt-to-escape frequency ($\omega_0 = 2\pi\nu_0$).[84,125] Taking the latter, the switching speed of the small-signal measurement inherently defines an energy demarcation which divides those defects that can emit charge and contribute to the capacitance from those that cannot,[63,92,125]

$$E_\omega = k_B T \ln\left(\frac{\omega_0}{\omega}\right) \tag{19}$$

where ω the applied angular frequency. As ω is swept from high to low frequencies, the demarcation energy is moved from below the Fermi-level, where no states can respond, to above the trap level(s), where all states respond (Fig. 21).[63,92] Note that only those states at the Fermi-level efficiently contribute and, in the low frequency limit, only those states between the mid-gap and Fermi-level will be probed.[92] An energetic profile of the tDOS can be found *via*,[92]

$$N_T(E_\omega) = -\frac{V_{bi}}{qW}\frac{dC}{d\omega}\frac{\omega}{k_B T}. \tag{20}$$

This profile is then fit with a Gaussian or exponential model and the characteristic trap parameters are extracted.

8.6. Drive-level transient spectroscopy (DLTS)

Also exploiting the depletion capacitance is DLTS. This powerful capacitance technique monitors transient changes in the capacitance signal induced by a voltage or optical pulse to study trap characteristics.[63] The technique was pioneered for crystalline semiconductors and later extended for amorphous materials.[126,127] Though the approach is slightly more in depth, the advantages lay in the extracted parameters. Along with trap band magnitudes, capture cross-section and activation energies, emission rates and trap types (*i.e.* majority or minority trap) can be easily examined.[63] It is worth noting, Sharma *et al.* have cautioned that, owing to the high resistivity and low hole mobility of some organic layers, DLTS may not be a suitable defect characterization technique for all organic applications (ref. 88 and 12 in ref. 88).

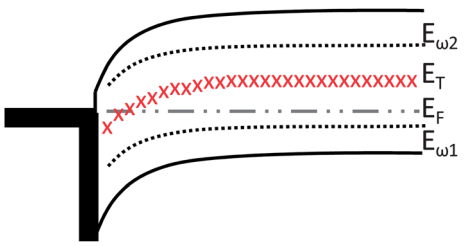

Fig. 21 Simplified p-type Schottky band diagram showing the CF experiment. E_F shows the Fermi-level energy, E_T the trap level, $E_{\omega 1}$ a high frequency demarcation where no states can respond and $E_{\omega 2}$ a low frequency demarcation where all states can respond.

8.7. Open-circuit impedance spectroscopy (IS)

Though the strict definition of impedance spectroscopy (IS) might include the previously discussed CF and CV measurements, we have kept their nomenclature separated in order to highlight a segregation in their use and analysis. Nonetheless, the IS method considered here is simply an application of the CF measurement at different, typical forward, voltage potentials. The results are typified by a Cole–Cole plot and can be used to study the density of photogenerated carriers, carrier mobility, carrier lifetime and the electron density of state.[35,77,99] In the latter, which is of particular interest here, the impedance characteristics are measured at open circuit conditions, where recombination precisely balances generation (Fig. 22).[99] To accomplish this, the photovoltaic device is illuminated at different intensities and a bias is applied to compensate the photovoltage. As such, the steady-state complex impedance examined is that of a chemical capacitance (ref. 35 and 77 and references therein), which is dominated by changes in the electron quasi Fermi-level (E_{Fn}) and defined by,

$$\frac{C_\mu}{A} = Lq^2\frac{dn}{dE_{Fn}} \tag{21}$$

where L is the active layer thickness.[99] Assuming a zero-temperature Fermi distribution,[99]

$$\frac{C_\mu}{A} = Lq^2 g(E_{Fn}). \tag{22}$$

Thereby, with small-scale movement of the polymer E_{Fp}, the fullerene DOS in the BHJ blend is readily obtained as E_{Fn} moves through the distribution at different illumination intensities (Fig. 22).

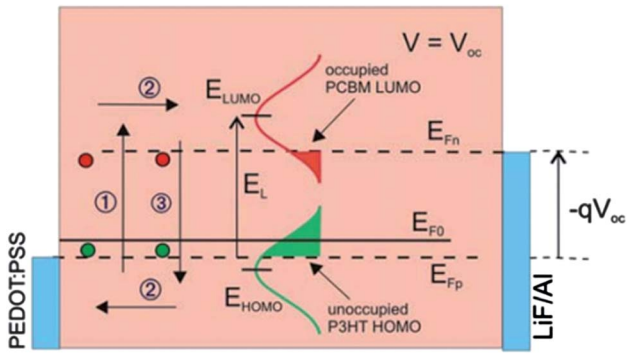

Fig. 22 Band structure of the P3HT:PCBM heterojunction in steady-state illumination under open-circuit conditions ($V = V_{oc}$). Main dynamic processes occurring in the blend layer: excess holes and electrons are photogenerated (1) into the P3HT HOMO and PCBM LUMO manifolds, respectively. Charge carriers diffuse along the diode bulk (2), and eventually recombine (3). Molecular orbitals spread in energy (DOS) following Gaussian shapes. The occupancy level of LUMO (HOMO) states is determined by competing photogeneration and recombination rates. This in turn governs the achievable V_{oc} which depends on the splitting of the quasi-Fermi levels, $-qV_{oc} = E_{Fn} - E_{Fp}$. The DOS centers are located at E_{LUMO} and E_{HOMO}, respectively. The relative position of the Fermi level in the dark E_{F0} is also indicated. Reprinted from publication ref. 99, Copyright [2010], with permission from Elsevier.

Acknowledgements

This article includes material from work supported by the National Science Foundation under Grant No. 1055930.

References

1 D. Yue, P. Khatav, F. You and S. B. Darling, *Energy Environ. Sci.*, 2012, **5**, 9163–9172.
2 B. A. Gregg, S. G. Chen and R. A. Cormier, *Chem. Mater.*, 2004, **16**, 4586–4599.
3 C. W. Tang, *Appl. Phys. Lett.*, 1986, **48**, 183–185.
4 G. Yu, J. Gao, J. C. Hummelen, F. Wudl and A. J. Heeger, *Science*, 1995, **270**, 1789–1791.
5 J. J. M. Halls, C. A. Walsh, N. C. Greenham, E. A. Marseglia, R. H. Friend, S. C. Moratti and A. B. Holmes, *Nature*, 1995, **376**, 498–500.
6 Z. He, C. Zhong, S. Su, M. Xu, H. Wu and Y. Cao, *Nat. Photonics*, 2012, **6**, 593–597.
7 T. Kirchartz, K. Taretto and U. Rau, *J. Phys. Chem. C*, 2009, **113**, 17958–17966.
8 L. Kaake, P. Barbara and X. Y. Zhu, *J. Phys. Chem. Lett.*, 2010, **1**, 628–635.
9 M. S. A. Abdou, F. P. Orfino, Y. Son and S. Holdcroft, *J. Am. Chem. Soc.*, 1997, **119**, 4518–4524.
10 S. Hoshino, M. Yoshida, S. Uemura, T. Kodzasa, N. Takada, T. Kamata and K. Yase, *J. Appl. Phys.*, 2004, **95**, 5088.
11 M. M. Erwin, J. McBride, A. V. Kadavanich and S. J. Rosenthal, *Thin Solid Films*, 2002, **409**, 198–205.
12 J. A. Carr, K. S. Nalwa, R. Mahadevapuram, Y. Chen, J. Anderegg and S. Chaudhary, *ACS Appl. Mater. Interfaces*, 2012, **4**, 2831–2835.
13 G. Dennler, C. Lungenschmied, N. S. Sariciftci, R. Schwödiauer, S. Bauer and H. Reiss, *Appl. Phys. Lett.*, 2005, **87**, 163501.
14 R. F. Salzman, J. Xue, B. P. Rand, A. Alexander, M. E. Thompson and S. R. Forrest, *Org. Electron.*, 2005, **6**, 242–246.
15 T. Matsushima, M. Yahiro and C. Adachi, *Appl. Phys. Lett.*, 2007, **91**, 103505.
16 W. L. Leong, G. C. Welch, L. G. Kaake, C. J. Takacs, Y. Sun, G. C. Bazan and A. J. Heeger, *Chem. Sci.*, 2012, **3**, 2103–2109.
17 F. C. Krebs, R. B. Nyberg and M. Jørgensen, *Chem. Mater.*, 2004, **16**, 1313–1318.
18 M. P. Nikiforov, B. Lai, W. Chen, S. Chen, R. D. Schaller, J. Strzalka, J. Maser and S. B. Darling, *Energy Environ. Sci.*, 2013, **6**, 1513–1520.
19 D. Lang, X. Chi, T. Siegrist, A. Sergent and A. Ramirez, *Phys. Rev. Lett.*, 2004, **93**, 76601.
20 D. Knipp and J. E. Northrup, *Adv. Mater.*, 2009, **21**, 2511–2515.
21 B. A. Gregg, *J. Phys. Chem. C*, 2009, **113**, 5899–5901.
22 K. S. Nalwa, R. C. Mahadevapuram and S. Chaudhary, *Appl. Phys. Lett.*, 2011, **98**, 093306.
23 D. Wang, N. Kopidakis, M. O. Reese and B. A. Gregg, *Chem. Mater.*, 2008, **20**, 6307–6309.
24 Z. Liang, A. Nardes, D. Wang, J. J. Berry and B. A. Gregg, *Chem. Mater.*, 2009, **21**, 4914–4919.
25 A. Hepp, N. Von Malm, R. Schmechel and H. Von Seggern, *Synth. Met.*, 2003, **138**, 201–207.
26 D. Wang, M. Reese, N. Kopidakis and B. A. Gregg, *Do the defects make it work? Defect engineering in pi-conjugated polymers and their solar cells*, 2008.
27 B. A. Gregg, *Soft Matter*, 2009, **5**, 2985–2989.
28 P. T. Landsberg, *Recombination in semiconductors*, Cambridge University Press, 2003.
29 J. Poortmans and V. Arkhipov, *Thin film solar cells: fabrication, characterization and applications*, Wiley, 2006.
30 R. A. Smith, *Semiconductors*, Cambridge University Press, Cambridge, UK, 1978.
31 M. Mandoc, F. Kooistra, J. Hummelen, B. de Boer and P. Blom, *Appl. Phys. Lett.*, 2007, **91**, 263505.
32 R. A. Street and M. Schoendorf, *Phys. Rev. B*, 2010, **81**, 205307.
33 S. R. Cowan, W. L. Leong, N. Banerji, G. Dennler and A. J. Heeger, *Adv. Funct. Mater.*, 2011, **21**, 3083–3092.
34 C. R. McNeill, I. Hwang and N. C. Greenham, *J. Appl. Phys.*, 2009, **106**, 024507.
35 G. Garcia-Belmonte, P. P. Boix, J. Bisquert, M. Lenes, H. J. Bolink, A. La Rosa, S. Filippone and N. Martín, *Sol. Cells*, 2010, **11**, 14.
36 J. Bhattacharya, R. Mayer, M. Samiee and V. Dalal, *Appl. Phys. Lett.*, 2012, **100**, 193501.
37 J. Schafferhans, A. Baumann, A. Wagenpfahl, C. Deibel and V. Dyakonov, *Org. Electron.*, 2010, **11**, 1693–1700.
38 G. Dicker, M. P. de Haas, J. M. Warman, D. M. de Leeuw and L. D. A. Siebbeles, *J. Phys. Chem. B*, 2004, **108**, 17818–17824.
39 P. P. Boix, G. Garcia-Belmonte, U. Munecas, M. Neophytou, C. Waldauf and R. Pacios, *Appl. Phys. Lett.*, 2009, **95**, 233302–233303.
40 B. A. Gregg, S. E. Gledhill and B. Scott, *J. Appl. Phys.*, 2006, **99**, 116104.
41 S. Jain, W. Geens, A. Mehra, V. Kumar, T. Aernouts, J. Poortmans, R. Mertens and M. Willander, *J. Appl. Phys.*, 2001, **89**, 3804–3810.
42 H. Hintz, H. Peisert, H. J. Egelhaaf and T. Chassé, *J. Phys. Chem. C*, 2011, **115**, 13373–13376.
43 E. Meijer, A. Mangnus, B. H. Huisman, G. t. Hooft, D. De Leeuw and T. Klapwijk, *Synth. Met.*, 2004, **142**, 53–56.
44 H. H. Liao, C. M. Yang, C. C. Liu, S. F. Horng, H. F. Meng and J. T. Shy, *J. Appl. Phys.*, 2008, **103**, 104506–104508.
45 C. K. Lu and H. F. Meng, *Phys. Rev. B: Condens. Matter Mater. Phys.*, 2007, **75**, 235206.
46 L. Lüer, H. J. Egelhaaf and D. Oelkrug, *Opt. Mater.*, 1998, **9**, 454–460.
47 A. Seemann, T. Sauermann, C. Lungenschmied, O. Armbruster, S. Bauer, H. J. Egelhaaf and J. Hauch, *Sol. Energy*, 2011, **85**, 1238–1249.
48 A. Aguirre, S. Meskers, R. Janssen and H. J. Egelhaaf, *Org. Electron.*, 2011, **12**, 1657–1662.
49 M. Chikamatsu, T. Taima, Y. Yoshida, K. Saito and K. Yase, *Appl. Phys. Lett.*, 2004, **84**, 127.
50 V. Arkhipov, P. Heremans, E. Emelianova and H. Baessler, *Phys. Rev. B: Condens. Matter Mater. Phys.*, 2005, **71**, 045214.
51 A. Liu, S. Zhao, S. B. Rim, J. Wu, M. Könemann, P. Erk and P. Peumans, *Adv. Mater.*, 2008, **20**, 1065–1070.

52 R. F. Pierret and G. W. Neudeck, *Advanced semiconductor fundamentals*, Addison-Wesley, Reading, MA, 1987.
53 L. Goris, A. Poruba, L. Hodakova, M. Vanecek, K. Haenen, M. Nesladek, P. Wagner, D. Vanderzande, L. De Schepper and J. Manca, *Appl. Phys. Lett.*, 2006, **88**, 052113.
54 T. Gotoh, S. Nonomura, S. Hirata and S. Nitta, *Appl. Surf. Sci.*, 1997, **113**, 278–281.
55 H. Habuchi, S. Nitta, D. Han and S. Nonomura, *J. Appl. Phys.*, 2000, **87**, 8580–8588.
56 V. Nikitenko, H. Heil and H. Von Seggern, *J. Appl. Phys.*, 2003, **94**, 2480.
57 J. Schafferhans, A. Baumann, C. Deibel and V. Dyakonov, *Appl. Phys. Lett.*, 2008, **93**, 093303.
58 S. Neugebauer, J. Rauh, C. Deibel and V. Dyakonov, *Appl. Phys. Lett.*, 2012, **100**, 263304.
59 B. G. Streetman and S. Banerjee, *Solid state electronic devices*, Prentice-Hall, 1995.
60 J. V. Li, A. M. Nardes, Z. Liang, S. E. Shaheen, B. A. Gregg and D. H. Levi, *Org. Electron.*, 2011, **12**, 1879–1885.
61 J. A. Carr, Y. Chen, M. Elshobaki, R. C. Mahadevapuram and S. Chaudhary, *Nanomater. Energy*, 2012, **1**, 8.
62 A. Campbell, D. Bradley, E. Werner and W. Brütting, *Synth. Met.*, 2000, **111**, 273–276.
63 J. Heath and P. Zabierowski, *Advanced Characterization Techniques for Thin Film Solar Cells*, 2011, pp. 81–105.
64 L. Kimerling, *J. Appl. Phys.*, 1974, **45**, 1839–1845.
65 D. Q. Feng, A. Caruso, Y. B. Losovyj, D. Shulz and P. Dowben, *Polym. Eng. Sci.*, 2007, **47**, 1359–1364.
66 H. Nicolai, M. Kuik, G. Wetzelaer, B. de Boer, C. Campbell, C. Risko, J. Brédas and P. Blom, *Nat. Mater.*, 2012, **11**, 882–887.
67 M. Lenes, S. W. Shelton, A. B. Sieval, D. F. Kronholm, J. C. K. Hummelen and P. W. M. Blom, *Adv. Funct. Mater.*, 2009, **19**, 3002–3007.
68 J. Schafferhans, C. Deibel and V. Dyakonov, *Adv. Energy Mater.*, 2011, **1**, 655–660.
69 A. Guerrero, P. P. Boix, L. F. Marchesi, T. Ripolles-Sanchis, E. C. Pereira and G. Garcia-Belmonte, *Sol. Energy Mater. Sol. Cells*, 2012, **100**, 185–191.
70 R. Könenkamp, G. Priebe and B. Pietzak, *Phys. Rev. B: Condens. Matter Mater. Phys.*, 1999, **60**, 11804.
71 A. Tapponnier, I. Biaggio and P. Gunter, *Appl. Phys. Lett.*, 2005, **86**, 112114.
72 P. A. Troshin, D. K. Susarova, Y. L. Moskvin, I. E. Kuznetsov, S. A. Ponomarenko, E. N. Myshkovskaya, K. A. Zakharcheva, A. A. Balakai, S. D. Babenko and V. F. Razumov, *Adv. Funct. Mater.*, 2010, **20**, 4351–4357.
73 A. Saeki, M. Tsuji and S. Seki, *Adv. Energy Mater.*, 2011, **1**, 661–669.
74 P. Yu, A. Migan-Dubois, J. Alvarez, A. Darga, V. Vissac, D. Mencaraglia, Y. Zhou and M. Krueger, *J. Non-Cryst. Solids*, 2012, **358**, 2537–2540.
75 C.-Y. Nam, D. Su and C. T. Black, *Adv. Funct. Mater.*, 2009, **19**, 3552–3559.
76 M. Glatthaar, N. Mingirulli, B. Zimmermann, T. Ziegler, R. Kern, M. Niggemann, A. Hinsch and A. Gombert, *Phys. Status Solidi A*, 2005, **202**, R125–R127.
77 G. Garcia-Belmonte, A. Munar, E. M. Barea, J. Bisquert, I. Ugarte and R. Pacios, *Org. Electron.*, 2008, **9**, 847–851.
78 P. P. Boix, J. Ajuria, I. Etxebarria, R. Pacios and G. Garcia-Belmonte, *Thin Solid Films*, 2011, **520**, 2265–2268.
79 V. Dyakonov, D. Godovsky, J. Meyer, J. Parisi, C. Brabec, N. Sariciftci and J. Hummelen, *Synth. Met.*, 2001, **124**, 103–105.
80 V. Dyakonov, I. Riedel, C. Deibel, J. Parisi, C. Brabec, N. Sariciftci and J. Hummelen, *Electronic Properties of Polymer-Fullerene Solar Cells*, 2002.
81 C. Deibel and A. Wagenpfahl, *Phys. Rev. B: Condens. Matter Mater. Phys.*, 2010, **82**, 207301.
82 R. Street, *Phys. Rev. B: Condens. Matter Mater. Phys.*, 2010, **82**, 207302.
83 M. M. Mandoc, W. Veurman, L. J. A. Koster, B. de Boer and P. W. Blom, *Adv. Funct. Mater.*, 2007, **17**, 2167–2173.
84 C. R. McNeill and N. C. Greenham, *Appl. Phys. Lett.*, 2008, **93**, 203310.
85 B. Ecker, J. C. Nolasco, J. Pallarés, L. F. Marsal, J. Posdorfer, J. Parisi and E. von Hauff, *Adv. Funct. Mater.*, 2011, **21**, 2705–2711.
86 J. Bisquert, G. Garcia-Belmonte, A. Munar, M. Sessolo, A. Soriano and H. J. Bolink, *Chem. Phys. Lett.*, 2008, **465**, 57–62.
87 S. K. Gupta, K. Dharmalingam, L. S. Pali, S. Rastogi, A. Singh and A. Garg, *Nanomaterials and Energy*, 2012, **2**(1), 42–58.
88 A. Sharma, P. Kumar, B. Singh, S. R. Chaudhuri and S. Ghosh, *Appl. Phys. Lett.*, 2011, **99**, 023301.
89 J. A. Carr and S. Chaudhary, *Appl. Phys. Lett.*, 2012, **100**, 213902–213904.
90 J. Nolasco, A. Sánchez-Díaz, R. Cabré, J. Ferré-Borrull, L. Marsal, E. Palomares and J. Pallarès, *Appl. Phys. Lett.*, 2010, **97**, 013305.
91 B. Yang, F. Guo, Y. Yuan, Z. Xiao, Y. Lu, Q. Dong and J. Huang, *Adv. Mater.*, 2013, **25**(4), 572–577.
92 T. Walter, R. Herberholz, C. Muller and H. Schock, *J. Appl. Phys.*, 1996, **80**, 4411–4420.
93 J. D. Cohen and D. V. Lang, *Phys. Rev. B: Condens. Matter Mater. Phys.*, 1982, **25**, 5321.
94 F. Reis, L. Santos, R. Bianchi, H. Cunha, D. Mencaraglia and R. Faria, *Appl. Phys. A: Mater. Sci. Process.*, 2009, **96**, 909–914.
95 D. Ray and K. Narasimhan, *J. Appl. Phys.*, 2008, **103**, 093711.
96 D. Mencaraglia, S. Ould Saad and Z. Djebbour, *Thin Solid Films*, 2003, **431**, 135–142.
97 M. Mingebach, C. Deibel and V. Dyakonov, *Phys. Rev. B: Condens. Matter Mater. Phys.*, 2011, **84**, 153201.
98 T. Kirchartz, W. Gong, S. A. Hawks, T. Agostinelli, R. C. I. MacKenzie, Y. Yang and J. Nelson, *J. Phys. Chem. C*, 2012, **116**, 7672.
99 G. Garcia-Belmonte, P. P. Boix, J. Bisquert, M. Sessolo and H. J. Bolink, *Sol. Energy Mater. Sol. Cells*, 2010, **94**, 366–375.
100 A. Yassar, L. Miozzo, R. Gironda and G. Horowitz, *Prog. Polym. Sci.*, 2013, **38**(5), 791–844.
101 B. A. Mattis, P. C. Chang and V. Subramanian, *Synth. Met.*, 2006, **156**, 1241–1248.

102 K. T. Nielsen, K. Bechgaard and F. C. Krebs, *Macromolecules*, 2005, **38**, 658–659.
103 K. T. Nielsen, K. Bechgaard and F. C. Krebs, *Synthesis*, 2006, 1639–1644.
104 J. E. Anthony, M. Heeney and B. S. Ong, *MRS Bull.*, 2008, **33**, 698–705.
105 B. Carsten, F. He, H. J. Son, T. Xu and L. Yu, *Chem. Rev.*, 2011, **111**, 1493–1528.
106 S. Olthof, S. Mehraeen, S. K. Mohapatra, S. Barlow, V. Coropceanu, J. L. Brédas, S. R. Marder and A. Kahn, *Phys. Rev. Lett.*, 2012, **109**, 176601.
107 Y. Zhang, B. de Boer and P. W. M. Blom, *Phys. Rev. B: Condens. Matter Mater. Phys.*, 2010, **81**, 085201.
108 T. Menke, D. Ray, J. Meiss, K. Leo and M. Riede, *Appl. Phys. Lett.*, 2012, **100**, 093304.
109 F. Li, M. Pfeiffer, A. Werner, K. Harada, K. Leo, N. Hayashi, K. Seki, X. Liu and X. D. Dang, *J. Appl. Phys.*, 2006, **100**, 023716.
110 P. P. Boix, J. Ajuria, I. Etxebarria, R. Pacios, G. Garcia-Belmonte and J. Bisquert, *J. Phys. Chem. Lett.*, 2011, **2**, 407–411.
111 C. Michelson, A. Gelatos and J. Cohen, *Appl. Phys. Lett.*, 1985, **47**, 412–414.
112 J. T. Heath, J. D. Cohen and W. N. Shafarman, *J. Appl. Phys.*, 2004, **95**, 1000.
113 J. A. Carr and S. Chaudhary, *J. Appl. Phys.*, 2013, **114**, 064509.
114 A. Kadashchuk, R. Schmechel, H. Von Seggern, U. Scherf and A. Vakhnin, *J. Appl. Phys.*, 2005, **98**, 024101–024109.
115 W. Graupner, G. Leditzky, G. Leising and U. Scherf, *Phys. Rev. B: Condens. Matter Mater. Phys.*, 1996, **54**, 7610.
116 Z. Fang, L. Shan, T. Schlesinger and A. Milnes, *Mater. Sci. Eng., B*, 1990, **5**, 397–408.
117 J. Steiger, R. Schmechel and H. Von Seggern, *Synth. Met.*, 2002, **129**, 1–7.
118 N. Von Malm, R. Schmechel and H. Von Seggern, *Synth. Met.*, 2002, **126**, 87–95.
119 V. Arkhipov, P. Heremans, E. Emelianova and G. Adriaenssens, *Appl. Phys. Lett.*, 2001, **79**, 4154–4156.
120 W. Hwang and K. Kao, *Solid-State Electron.*, 1972, **15**, 523–529.
121 P. Mark and W. Helfrich, *J. Appl. Phys.*, 1962, **33**, 205–215.
122 W. Hwang, *Solid-State Electron.*, 1976, **19**, 1045–1047.
123 H. Nicolai, M. Mandoc and P. Blom, *Phys. Rev. B: Condens. Matter Mater. Phys.*, 2011, **83**, 195204.
124 S. S. Hegedus and W. N. Shafarman, *Prog. Photovoltaics*, 2004, **12**, 155–176.
125 S. S. Hegedus and E. Fagen, *J. Appl. Phys.*, 1992, **71**, 5941–5951.
126 D. Lang, *J. Appl. Phys.*, 1974, **45**, 3023–3032.
127 D. V. Lang, J. D. Cohen and J. P. Harbison, *Phys. Rev. B: Condens. Matter Mater. Phys.*, 1982, **25**, 5285.